We are IntechOpen,
the world's leading publisher of
Open Access books
Built by scientists, for scientists

4,800
Open access books available

122,000
International authors and editors

135M
Downloads

Our authors are among the

154
Countries delivered to

TOP 1%
most cited scientists

12.2%
Contributors from top 500 universities

CLARIVATE ANALYTICS

BOOK CITATION INDEX

INDEXED

WEB OF SCIENCE™

Selection of our books indexed in the Book Citation Index
in Web of Science™ Core Collection (BKCI)

Interested in publishing with us?
Contact book.department@intechopen.com

Numbers displayed above are based on latest data collected.
For more information visit www.intechopen.com

Photoelectron and Photosensitization Properties of Silicon Nanocrystal Ensembles

Elizaveta A. Konstantinova[1,2], Vyacheslav A. Demin[2]
and Pavel K. Kashkarov[1,2]
[1]Moscow State University, Moscow
[2]Russian Research Center Kurchatov Institute, Moscow
Russia

1. Introduction

Due to their unique properties, silicon nanocrystals get wide applications in various fields of science and engineering (Bisi et al., 2000). Recently, it has been revealed that photoexcitation of nanocrystals in microporous silicon (micro-PS) layers leads to the generation of singlet oxygen on the surface of the samples (Kovalev et al., 2002). It is known that the ground state of the oxygen molecule is represented by the triplet state ($^3O_2$, where the superscript indicates the spin multiplicity; the total spin of the triplet molecule is $S_{TO}= 1$). During energy absorption, the oxygen molecule transforms into an excited singlet state ($^1O_2$, $S_{SO}= 0$) (Halliwell & Gutteridge, 1999). In this state, the oxygen molecule exhibits the highest reactivity and enters into oxidation reactions with many substances. This property of singlet oxygen $^1O_2$ is widely used in biomedicine and, in particular, in photodynamic therapy of cancer (Halliwell & Gutteridge, 1999). It should be noted that direct excitation of molecular oxygen from the triplet state to the singlet one is forbidden by the selection rules for the orbital and spin quantum numbers. In order to transform molecular oxygen into the singlet state, it is common practice to use organic dyes that serve as photosensitizers (Kumar et al., 2009). An important property of micro-PS lies in the fact that upon photoexcitation of silicon nancrystals excitons are generated at rather high concentrations (the quantum yield of exciton photoluminescence reaches a few percent (Bisi et al., 2000)). It has been demonstrated that the energy can be effectively transferred from excitons to $^3O_2$ molecules adsorbed on the surface of silicon nanocrystals with the subsequent transformation of these molecules into an excited state (Gross et al., 2003; Kovalev et al., 2002). Therein lies the essence of the mechanism of photosensitization of molecular oxygen. The energy exchange between excitons and $^3O_2$ molecules occurs through the exchange of electrons (Gross et al., 2003) (the Dexter mechanism (Dexter, 1953)). Compared to organic dyes, the use of micro-PS as a photosensitizer of molecular oxygen offers a number of advantages, for example, the relatively simple and available technique for synthesizing this material and its nontoxicity. Evidently, it is important to determine the concentration of the generated singlet oxygen for the practical use of this effect. In this work, we used electron paramagnetic resonance (EPR) spectroscopy for this purpose. EPR spectroscopy allows us to study the interaction of spin centers on the surface of silicon nanocrystals (silicon dangling bonds) with the paramagnetic

molecules of triplet oxygen and thus to measure a decrease of their relative amount. The EPR-diagnostics of the $^1O_2$ oxygen generation, suggested in the present work, is based on the change in the spin–lattice (T_1) and spin–spin (T_2) relaxation times of spin centers, i.e., silicon dangling bonds (the so-called P_b centers (Bisi et al., 2000)). In this respect, in the present study, these times were measured by the pulsed EPR technique. The results obtained were confirmed by directly measuring the change in the amount of $^3O_2$ oxygen upon photoexcitation of micro-PS with the use of EPR technique in the Q band. It should be noted that the photosensitization of O_2 molecules on the micro-PS surface is one of the possible channels for nonradiative recombination of excitons in silicon nanostructures. Therefore, to achieve the maximum efficiency of $^1O_2$ generation in microporous silicon layers, it is important to comprehensively study the transfer and scattering of the excited silicon nanocrystals energy and to determine the characteristic times of these processes. To solve this problem, we analyze the decay kinetics of the photoluminescence (PL) of silicon nanocrystals (nc-Si) in micro-PS layers. The PL intensity of such samples is known to be well described by the so-called stretched exponent (Maly et al., 1996)

$$I_{PL} = I_{PL}^{(0)} \exp\left(-(t/\tau)^\beta\right), \tag{1}$$

where τ is the average PL lifetime and β is the nonexponentiality parameter. The values of τ and β depend on the excitation wavelength λ, temperature (Pavesi & Ceschini, 1993), and intensity and some other parameters (Chen et al., 1992) and are τ = 5–50 μs and β = 0.5–0.7 for PS samples with porosity P=70%. Note that Eq. (1) describes the PL relaxation kinetics in both ensembles of interconnected nc-Si in porous silicon layers (Mihalcescu et al., 1996; Pavesi & Ceschini, 1993) and other solid-state nanostructures, such as closely spaced (1–2 nm) nc-Si in a SiO_2 matrix (nc-Si/SiO_2) (Germanenko et al., 2001; Kanemitsu, 1996), CdSe–ZnSe superlattices (Chen et al., 1992), InGaN layered structures (Pophristic et al., 1998), and nanoporous SiGe solid solutions (Lebib et al., 1999). Numerous attempts were made to explain the causes of the stretched exponent of PL relaxation in the systems given above. For example, the authors of (Chen et al., 1992; Kanemitsu, 1996) relate this character of luminescence drop to the presence of disordered regions in these objects, which can be caused by a shape distribution of nanocrystals or a variation in their spatial arrangement. These factors induce a scatter of the recombination energies and probabilities of electron–hole pairs, which is likely to result in luminescence kinetics of type (1). Other researchers (Germanenko et al., 2001; Linnros et al., 1999) assume that the distortion of a luminescence monoexponential decrease is mainly caused by energy transfer between neighboring nanocrystals. This energy transfer can occur because of exciton migration from smaller to larger nanocrystals owing to a smaller energy gap in the latter nanocrystals. Thus, the exciton lifetime depends on the transfer rate; as a result, the kinetics of PL intensity drop "stretches". This assumption is supported by the study of the PL time characteristics of nc-Si ensembles separated by sufficiently thick (about 5 nm) spatial SiO_2 barriers (Vinciguerra, et al., 2000). In this case, nc-Si crystals are supposed to be well isolated; therefore, no energy exchange occurs between them and the lifetime is constant for nc-Si of a given size. Indeed, the PL kinetics detected in such systems turns out to be monoexponential with a characteristic time of 0.2–0.8 ms (Vinciguerra, et al., 2000). However, recent theoretical investigation (Chen, 2003) predicts a stretched exponent for PL kinetics even for individual (isolated) nanocrystals in the case where the rate of trapping of photoexcited charge carriers is higher than the rate of their recombination. Note that Chen (Chen, 2003) assumed that

nonradiative carrier capture centers should occur in every nc-Si. However, this assumption was not supported experimentally for luminescent PS samples, since EPR spectroscopy data demonstrate that the number of defects in 1 cm^3 (about 10^{17}) is much smaller than the number of nc-Si crystals in this volume (about 10^{19}–10^{20} or 10^{21} in the case of a fractal PS structure (Moretti et al., 2007; Nychyporuk et al., 2005)). Thus, most nc-Si do not have trapping sites, which requires an alternative explanation for the nonexponential kinetic curves of PL decay. Therefore the purpose of this work is (i) to experimentally investigate the process of singlet oxygen generation in nc-Si ensembles using electron paramagnetic resonance and photoluminescence spectroscopy and (ii) to theoretically study the PL decrease kinetics and the steady-state PL intensity of ensembles of nc-Si with allowance for exciton migration–assisted energy transfer in them, and (iii) to compare the results obtained in terms of the developed theory with the experimental data on the luminescence and photosensitization properties of nc-Si ensembles.

2. Sample preparation and experimental technique

Silicon nanocrystals in the PS layers were formed by a standard method of the electrochemical etching of silicon single crystals in a solution based on hydrofluoric acid: HF(48%) : C$_2$H$_5$OH=1 : 1 (e.g., see the review (Bisi et al., 2000)). The *p*-type crystalline silicon with the (100) surface orientation and the resistivity ρ=10…20 Ω cm and 10…20 mΩ cm was used as a substrate for micro-PS and meso-PS. The current density was 50 mA/cm^2 (micro-PS1 and meso-PS) and 70 mA/cm^2 (micro-PS2), the etching time was 60 min. After the completion of the pore formation process, PS layer was lifted from the substrate by a short-time increase in the current density to 700 mA/cm^2. The sample thickness measured with an optical microscope was 50 µm. Porosity of the samples was determined gravimetrically and was approximately 70 % for micro-PS1 and meso-PS samples, and 85 % for micro-PS2 samples. As determined by transmission electron microscopy, the average size of the nanocrystals was about 2–4 nm (micro-PS) and ~10 nm (meso-PS). A part of micro-PS samples were dried in air (PS1 and PS2 samples). Upon drying in air at room temperature, the PS films were failed by the surface tension force of water and transformed into granules with a lateral size of about 0.5 mm (coarsegrained (CG) PS). Fine-grained (FG) PS was prepared by mechanical milling in air of a CG PS powder placed in an ampule with quartz balls on a vibratory mill at a vibration frequency of 17 Hz and an amplitude of 7 mm for 2 min.

The EPR measurements were performed on a Bruker ELEXSYS-580 EPR spectrometer (operating frequency is 9.5 and 35 GHz, X- and Q-band, recpectively). Pulsed EPR measurements were made at the regime of "spin-echo" (time resolution ~5 ns). The admission of oxygen and the subsequent evacuation to the residual pressure $p \sim 10^{-5}$ mbar were performed "in situ" using oil-free vacuum equipment. For Q-band measurements soldered ampoules with PS in oxygen ambient were used because of technical features. The samples were illuminated with light from a halogen lamp at the maximum intensity I_{exc} ~2 W/cm^2 immediately in the resonator of the EPR spectrometer.

The PL of the PS samples were excited by nitrogen laser radiation with a wavelength of 337 nm at pulse duration of 10 ns and pulse energy of 10 µJ. PL spectra were measured on a Solar TII spectrometer equipped with a Hamamatsu MS-101H CCD camera. PL kinetics

were recorded with an MDR-12 monochromator, Hamamatsu R237 photomultiplier tube, and an Agilent 54642A digital oscilloscope.

The experiments were carried out at room temperature.

3. Results and discussion

3.1 Investigation of the EPR spectra of silicon nanocrystalls in the PS1 layers in vacuum, nitrogen and oxygen

Figure 1a shows the EPR spectra of micro-PS samples in oxygen in the dark and under illumination, which were measured at the low power P_{mw} = 0.64 mW of incident microwave radiation. The parameters of the observed EPR signal are characteristic of P_b-centers, which are the dangling bonds of silicon at the Si/SiO_2 interface (Bisi et al., 2000; Cantin et al., 1995).
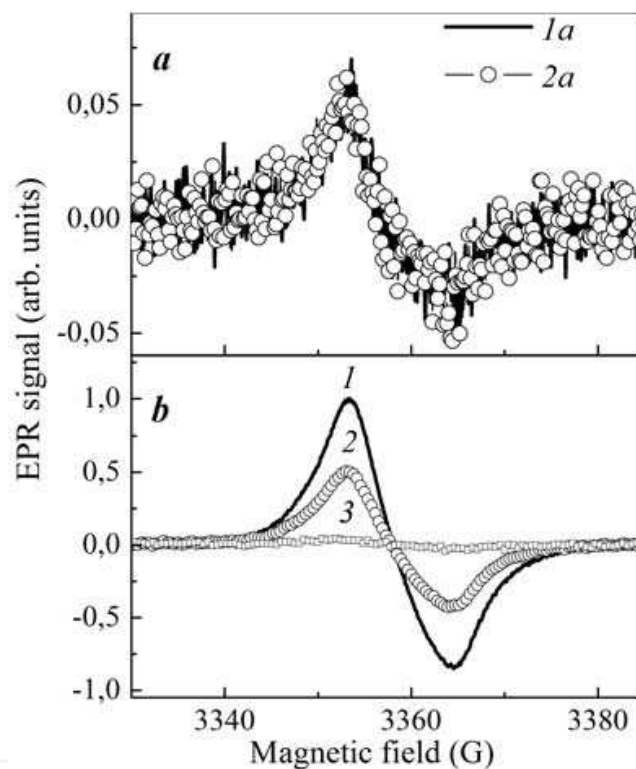

Fig. 1. (a) EPR spectra of PS measured at P_{mw} =0.64 mW in an oxygen atmosphere (*1a*) in the dark and (*2a*) under illumination. (b) EPR spectra of PS in an oxygen atmosphere (*1*) in the dark and (*2*) under illumination with the intensity I_{exc} = 650 mW/cm² or (*3*) in a vacuum

As can be seen in Fig. 1a, a noticeable change in the EPR signal amplitude of micro-PS in oxygen did not occur under illumination (curve *2a*), as compared with that in the dark (curve *1a*). At the same time, a considerable variation in the EPR signal amplitude of micro-PS under analogous conditions was detected at P_{mw} =200 mW (Fig. 1b; curves *1* and *2*). It is well known that, at a sufficiently high intensity of microwave radiation its absorption by P_b centers was saturated; this manifested itself in a decrease in the EPR signal amplitude (Cantin et al., 1995). This effect was observed in our measurements performed with micro-PS in a vacuum (Fig. 1b, curve *3*). Note that the relaxation of P_b-centers from an excited state

to the ground state occurred by energy transfer to crystal lattice phonons in the case of micro-PS samples in a vacuum. At the same time for micro-PS in an oxygen atmosphere, the magnetic dipoles of $^3O_2$ molecules adsorbed on the surface of silicon nanocrystals interacted with the magnetic moments of excited P_b-centers to induce their rapid relaxation to the ground state. Consequently, the relaxation time of P_b-centers for micro-PS in an oxygen atmosphere decreased; the saturation effect of microwave absorption weakened; and, as a result, the EPR signal amplitude considerably increased (Fig. 1b, curve *1*). The photosensitization of oxygen molecules occurred under the illumination of micro-PS layers placed in an oxygen atmosphere; consequently, the concentration of $^3O_2$ molecules decreased. In turn, this caused an increase in the relaxation time of P_b-centers; as a result of this, the EPR signal amplitude decreased (Fig. 1b, curve 2). It should be noted that the change in the EPR signal amplitude upon photoexcitation of PS is almost completely reversible in switching on–switching off cycles if the defect formation under illumination is reduced to a minimum. The samples under investigation satisfy this condition, because they were preliminarily oxidized upon illumination in air for several minutes, which resulted in a considerable decrease in the defect generation rate.

In order to confirm the decisive role of oxygen in the decrease of the EPR signal amplitude upon photoexcitation of nc-Si, we measured the EPR spectra of micro-PS in an atmosphere of nitrogen because of N_2 molecules are diamagnetic (Fig. 2). As can be seen in Fig.2, a noticeable change in the EPR signal amplitude of micro-PS in nitrogen ambient did not occur under illumination (curve 2), as compared with that in the dark (curve 1). The amplitude of both spectra is small because of saturation effect. Therefore the relaxation of spins takes place only throw spin-lattice relaxation canal, the spin-spin relaxation is suppressed because of diamagnetic nature of N_2 molecules. Therefore namely triplet oxygen molecules are responsible for the effective spin relaxation process and an elimination of saturation effect.
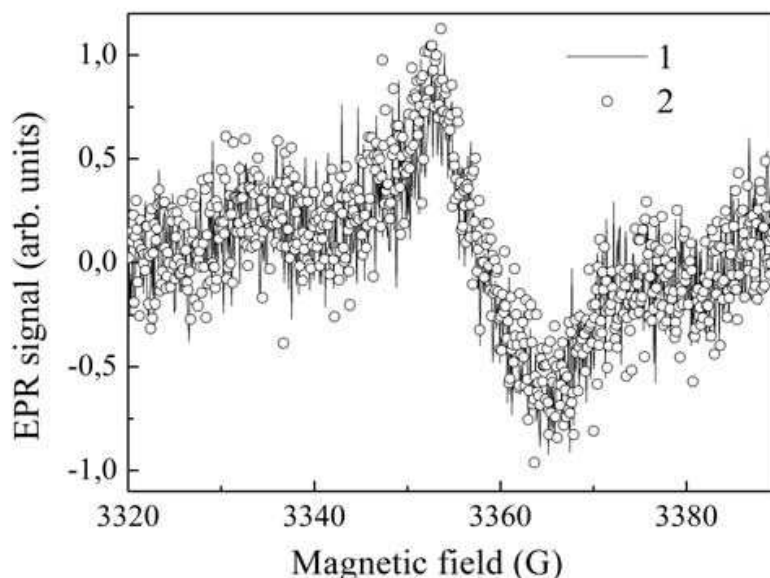

Fig. 2. EPR spectra of micro-PS in an nitrogen atmosphere: (1) in the dark and (2) under illumination. Experimental conditions: P_{mw} =200 mW, I_{exc} =650 mW/cm^2, and p_{O_2} =1 bar.

Control experiments for meso-PS show that there is no change in EPR spectra amplitude of meso-PS under illumination of the samples in oxygen ambient (Fig.3). This fact points out an absence of singlet oxygen generation effect and confirms the decisive role of excitons in energy transfer process from photoexcited excitons in nc-Si to oxygen molecules adsorbed on their surface. Indeed, the average size of nanocrystals in meso-PS layers is approximately 10 nm. In such systems the exciton binding energy is small in comparison with thermal energy at room temperature (26 meV).
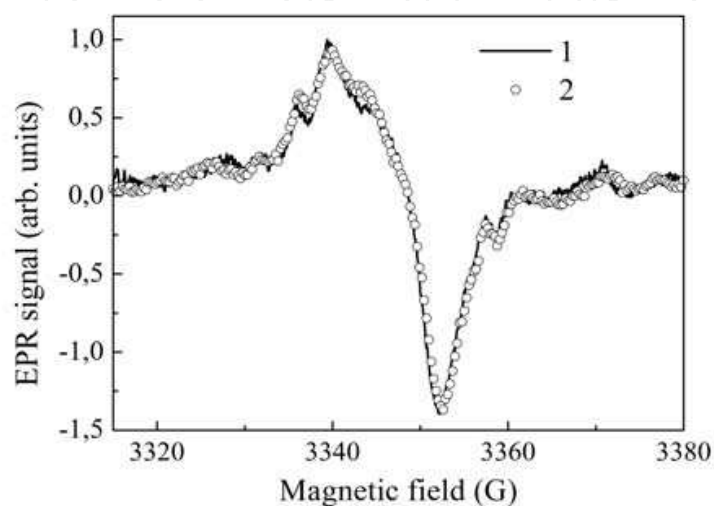

Fig. 3. EPR spectra of meso-PS in oxygen: (1) in the dark and (2) under illumination. Experimental conditions: P_{mw} =200 mW, I_{exc} = 650 mW/cm², and p_{O_2} = 1 bar.

The above data were obtained at high microwave powers P_{mw}. In order to evaluate the limits of applicability of the EPR technique in the study of the generation of singlet oxygen upon photoexcitation of silicon nanocrystals, let us analyze the influence of the microwave power on the EPR signal amplitude. The dependences of the EPR signal amplitude on the square root of the microwave radiation power $I_{EPR}(\sqrt{P_{mw}})$ are plotted in Fig. 4. It can be seen from this figure that the dependences $I_{EPR}(\sqrt{P_{mw}})$ obtained in vacuum and oxygen under illumination and in the dark coincide at low microwave powers ($P_{mw} \leq 0.5$ mW) and differ substantially at high microwave powers due to the saturation effect. Actually, at low microwave powers P_{mw}, the probability W of induced resonance transitions between the Zeeman energy levels per unit time is so low that, even in the case of the electron–phonon mechanism of relaxation of the P_b center (dominant in vacuum), its characteristic lifetime in the excited state is shorter than the characteristic time 1/W of absorption of a microwave photon. Consequently, at low microwave powers P_{mw}, the saturation effect is absent and, correspondingly, the EPR signal amplitudes are identical for micro-PS in vacuum and the oxygen atmosphere irrespective of the illumination (Fig. 4).

Consequently, at low microwave powers P_{mw}, the saturation effect is absent and, correspondingly, the EPR signal amplitudes are identical for micro-PS in vacuum and the oxygen atmosphere irrespective of the illumination (Fig. 4). The last circumstance along with the reversibility of the amplitude of the EPR spectrum after illumination is switched off is an additional argument indicating that the above decrease in the amplitude at high
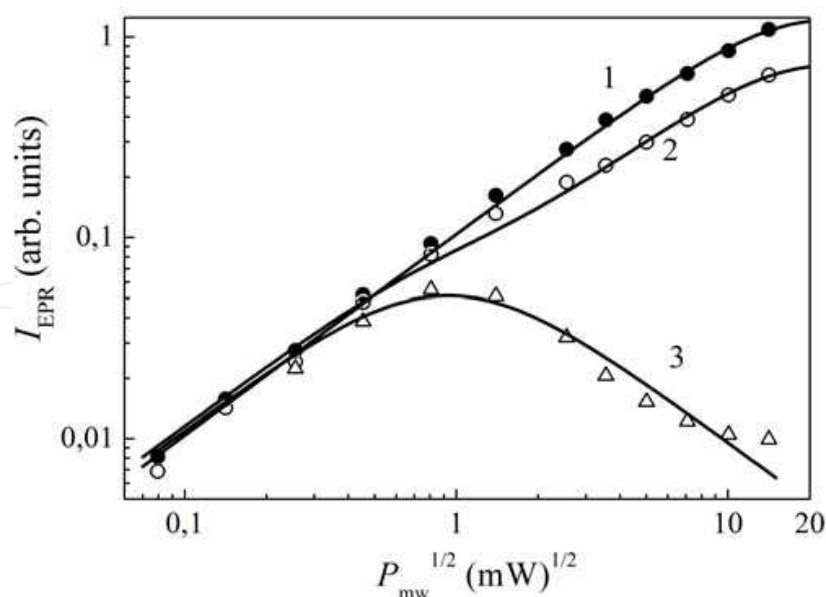
Fig. 4. Saturation curves for micro-PS in oxygen (p_{O_2} =1 bar): (1) in the dark, (2) under illumination, and (3) in vacuum (p_{O_2} =10⁻⁶ bar). The approximation dependences were obtained in the framework of the Bloch theory with due regard for the specific features of the detection system. The errors coincide with the sizes of experimental points.

microwave powers P_{mw} (Fig. 1) is not associated with the decrease in the number of spin centers in the sample. However, as was noted above, the decrease in the concentration of triplet oxygen either upon evacuation or in the course of photosensitization of oxygen molecules leads to an increase in the characteristic relaxation times of P_b centers and, as a consequence, to a decrease in the absorption of the microwave power. Indeed, the saturation curve for micro-PS in oxygen under illumination (Fig. 4, curve 2) lies lower than that obtained under dark conditions (Fig. 4, curve 1) (effect of generation of ¹O₂ molecules), and the saturation curve for the samples in vacuum (Fig. 4, curve 3) is characterized by a lower amplitude as compared to curve 2, passes through a maximum, and falls off with an increase in the microwave power P_{mw} (Fig. 4). In order to explain this behavior of the dependences $I_{EPR}\left(\sqrt{P_{mw}}\right)$, we invoke the Bloch theory, according to which the shape of the absorption line g(ω) in the EPR spectrum is described by the following relationship (Carrington & McLachlan, 1979):

$$g(\omega) = \frac{H_1^2 T_2}{s + T_2^2 (\omega - \omega_0)^2},$$ (2)

where H_1 is the amplitude of the magnetic field strength of the microwave wave, ω_0 is the frequency of the EPR transition, $s = 1 + \gamma^2 H_1^2 T_1 T_2$ is the so-called saturation factor, and γ is the electron gyromagnetic ratio. It should be noted that the dependences of the EPR signal amplitude on the microwave radiation power are shown in Fig. 4 in the form $I_{EPR}\left(\sqrt{P_{mw}}\right)$ universally accepted in EPR spectroscopy (see, for example, (Laiho et al., 1994; Poole & Horacio, 1987)). As can be seen from Fig. 4, the dependences $I_{EPR}\left(\sqrt{P_{mw}}\right)$ exhibit a linear behavior due to the linearity of the detection of the EPR signal with respect to the field in the

microwave wave incident on the detector (Schottky diode) over the entire range of the microwave radiation powers used [11]. Then, the dependence of the diode current j on the microwave power that is incident on the diode and equal to the difference between the quantities P_{mw} and ΔP_{mw} (the power absorbed by the sample in the cavity) can be written in the form

$$j \propto \sqrt{P_{mw} - \Delta P_{mw}} \approx \sqrt{P_{mw}} - \frac{\Delta P_{mw}}{2\sqrt{P_{mw}}} \tag{3}$$

because $\Delta P_{mw} << P_{mw}$ (Poole & Horacio, 1987). By using expressions (2) and (3), the obvious relationship $\sqrt{P_{mw}} \propto H_1$, and the fact that $\Delta P_{mw} \propto g(\omega)$ (Carrington & McLachlan, 1979), we obtain the expression for the recorded EPR signal $I(\omega; \omega_0)$ in the following form:

$$I(\omega; \omega_0) \propto \frac{\Delta P_{mw}}{\sqrt{P_{mw}}} \propto \frac{H_1 T_2}{s + T_2^2 (\omega - \omega_0)^2} \tag{4}$$

Taking into account that the EPR spectrum, as a rule, is recorded in the form of the first derivative $I'(\omega; \omega_0)$ of expression (4) with respect to ω, we have

$$I'(\omega; \omega_0) \propto -\frac{2H_1 T_2^3 (\omega - \omega_0)}{\left[s + T_2^2 (\omega - \omega_0)^2 \right]^2} . \tag{5}$$

The width and the amplitude of the EPR spectrum determined by formula (5) are represented in the form

$$\Delta \omega_{pp} = \frac{2}{T_2} \sqrt{\frac{s}{3}} , \tag{6a}$$

$$I_{EPR} = \frac{9}{4\sqrt{3}} \frac{H_1 T_2^2}{\left(1 + \gamma^2 H_1^2 T_1 T_2\right)^{3/2}} = \frac{a\sqrt{P_{mw}}}{\left(1 + bP_{mw}\right)^{3/2}} , \tag{6b}$$

where the parameters a and b determine the position of the maximum in the dependence $I_{EPR}\left(\sqrt{P_{mw}}\right)$; that is,

$$P_{mw}^{max} = \frac{1}{2b} , \quad I_{EPR}^{max} = \frac{2a}{\sqrt{27b}} . \tag{7}$$

Relationships (2) and (4)–(6) are valid in the case of a homogeneous broadening of the EPR line due to a finite lifetime of spin centers in the excited state. However, the EPR line of porous silicon is inhomogeneously broadened and can be described by the Gaussian distribution (Carrington & McLachlan, 1979)

$$N(\Delta\omega) = \frac{T_2^*}{\sqrt{2\pi}} \exp\left[-\left(\frac{\Delta\omega T_2^*}{2} \right)^2 \right] ,$$

where $\dfrac{1}{T_2^*} = \sqrt{\langle (\Delta\omega)^2 \rangle}$ is the root-mean-square deviation of the Larmor precession frequency in the volume of the sample. Then, the experimentally observed EPR spectrum can be written in the following from (Carrington & McLachlan, 1979):

$$I^{real}(\omega;\omega_0) = \int_{-\infty}^{+\infty} I(\omega;\omega_0 + \Delta\omega)N(\Delta\omega)d\Delta\omega, \qquad (8)$$

where $I(\omega;\omega_0 + \Delta\omega)$ is a homogeneously broadened spectrum defined by expression (4). An analysis of relationship (8) demonstrates that changes in the characteristics (for example, the amplitude) of the spectrum $I(\omega;\omega_0 + \Delta\omega)$ result in the corresponding changes in the characteristics of the spectrum $I^{real}(\omega;\omega_0)$; i.e., there is a one-to-one correlation between these spectra. Therefore, in order to avoid complications of calculations, the dependences $I_{EPR}\left(\sqrt{P_{mw}}\right)$ for micro-PS in vacuum and oxygen in the dark were approximated by expression (6b) that involves the fitting parameters a and b and holds true for the homogeneously broadened spectrum. In this case, the calculated curves and the experimental data are in satisfactory agreement (Fig. 4). The fitting parameters were determined to be a_v=0.09 relative units and b_v=0.4 mW^{-1} for the sample in vacuum and a_d=0.10 relative units and b_d = 1.1 × 10^{-3} mW^{-1} for the sample in the oxygen atmosphere under the dark conditions. According to formulas (7), the saturation curve $I_{EPR}\left(\sqrt{P_{mw}}\right)$ reaches a maximum at P_{mw}^{max} = 1.25 mW for micro-PS in vacuum and P_{mw}^{max} = 450 mW for porous silicon in oxygen. The dependences $I_{EPR}\left(\sqrt{P_{mw}}\right)$ for the samples of PS in oxygen under illumination were approximated by the sum of the saturation curves for PS in the oxygen atmosphere in the dark and in vacuum (Fig. 4): $I_{EPR}^{light} = \alpha \cdot I_{EPR}^{vac} + \beta \cdot I_{EPR}^{dark}$. In this expression, the quantity α determines the fraction of nanocrystals involved in the photosensitization of oxygen and the quantity β determines the fraction of nanocrystals that do not participate in this process ($\alpha + \beta$ = 1). Actually, nc-Si with sizes that do not exceed 2–4 nm are electron donors for triplet oxygen molecules, because these nanocrystals contain excitons due to the quantum size effect. Therefore, their surface under illumination is predominantly covered by $^1O_2$ molecules that do not contribute to the paramagnetic relaxation. The other part of nanocrystals (with larger sizes), as in the case of meso-PS (see above), do not make a contribution to the photosensitization of oxygen. This is equivalent to the relaxation of P_b centers in the atmosphere of $^3O_2$ molecules under the dark conditions. It follows from the aforesaid that the quantity α also determines the percentage of oxygen molecules transforming from the triplet state to the singlet state. The best approximation is achieved at α =0.41 and β =0.59. This means that, in our case, approximately 41% of the total number of oxygen molecules transform into the singlet state. The quantity α is conveniently expressed through the experimental data. Indeed, since $\alpha + \beta$ =1, we have

$$I_{EPR}^{light} = \alpha \cdot I_{EPR}^{vac} + (1-\alpha) \cdot I_{EPR}^{dark}$$

and, hence,

$$\alpha = \frac{I_{EPR}^{dark} - I_{EPR}^{light}}{I_{EPR}^{dark} - I_{EPR}^{vac}} . \tag{9}$$

The quantity α calculated from formula (9) at high microwave powers P_{mw} corresponds to the fraction of oxygen molecules that transform into the singlet state upon illumination of micro-PS layers. For example, by using the data presented in Fig. 4, we obtain α =0.42 at $P_{mw}^{\max}$ = 200 mW, which almost completely coincides with the value α = 0.41 determined by approximating the experimental data from Fig. 4 with use of the theoretical curves calculated from relationship (6b). Therefore, a considerable fraction (approximately 40%) of the molecules of triplet oxygen can transform into the singlet state upon photoexcitation of nc-Si. Evidently, the efficiency of generation of $^1O_2$ molecules depends on the amount of $^3O_2$ molecules that surround a silicon nanocrystal. Figure 5a shows the dependence of EPR signal amplitudes on the pressure of oxygen (p) for PS layers in the dark and under illumination. The curve for the sample in oxygen under illumination is also described by $I_{EPR}^{light} = \alpha \cdot I_{EPR}^{vac} + \beta \cdot I_{EPR}^{dark}$; however, in this case, the quantities α and β are also functions of p. Indeed, the time of energy transfer from an exciton to the $^3O_2$ molecule shortened as the concentration of oxygen molecules surrounding a nanocrystal was increased (Gross et al., 2003). In this case, the relaxation time of $^1O_2$ remained unchanged (direct singlet–triplet energy exchange between oxygen molecules is spin forbidden). Consequently, the fraction of $^1O_2$ molecules adsorbed on the surface of silicon nanocrystals increased. At the same time, this fraction depends on the quantity α (see above), which is responsible for the dependence of α on p. Using Eq. (9), we can express the value of α in terms of experimental data shown in Fig. 5a. The amplitude of an EPR signal at p = 10^{-5} mbar was chosen as I_{EPR}^{dark}. The dependence of the fraction of photosensitized $^1O_2$ molecules on p thus obtained can be directly converted into the concentration of $^1O_2$ molecules (N_{SO}) taking into account the initial triplet oxygen concentration in silicon pores, which is equal to $2.7 \cdot 10^{19}$ cm^{-3} at p_{O2} =1 bar (the Avogadro number divided by the molar volume). Figure 5b shows this result.

An increase in the intensity of illumination of porous silicon nanocrystals caused an increase in amount of $^1O_2$ molecules photosensitized on the surface of nc-Si (Gross et al., 2003) As a result of this, the EPR signal amplitude decreased (Fig. 6). In this case, a sharp decrease in the value of I_{EPR} was observed up to I_{exc}=600 mW/cm^2; as I_{exc} was further increased, I_{EPR} reached an approximately constant value. The latter was likely due to the fact that, at the specified value, the predominant fraction of oxygen molecules that covered a nanocrystal occurred in a singlet state. Figure 6 also shows the dependence of N_{SO} on I_{exc}, as calculated using Eq. (9) with consideration for the initial concentration of triplet oxygen.

3.2 Investigation of the photosensitization of oxygen molecules by the pulsed EPR technique

The EPR diagnostics of the generation of $^1O_2$ oxygen molecules in ensembles of silicon nanocrystals (considered in the preceding section) is based on a change in the relaxation times of spin centers. In this respect, the relaxation times T_1 and T_2 of spin centers in the samples under investigation were measured by the pulsed EPR technique based on the spin echo phenomenon (Hahn, 1950). It should be noted that, since the relaxation time T_1 characterizes the return of the net magnetization component parallel to the constant
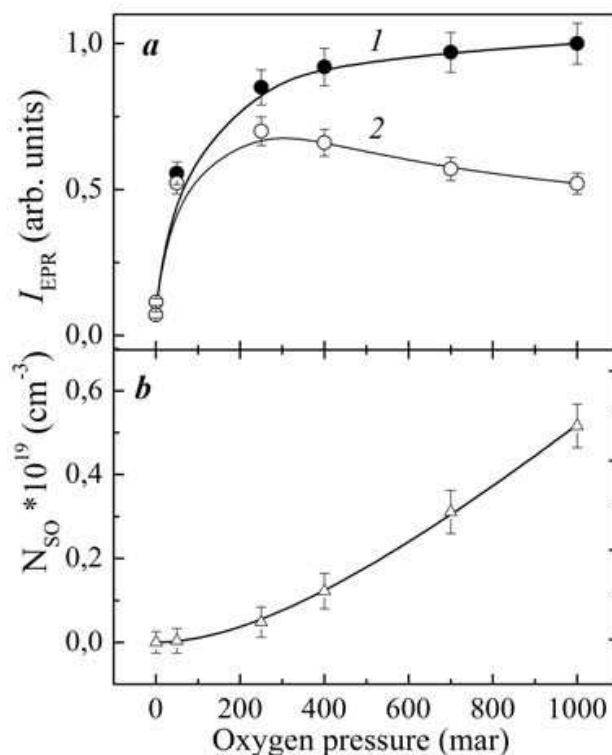
Fig. 5. (a) The amplitude of the EPR spectra of micro-PS samples vs. p_{O_2} (*1*) in the dark and (*2*) under illumination. (b) The concentration of $^1O_2$ molecules photosensitized in the PS layers vs. p_{O_2}. The parameters are I_{exc}=650 mW/cm^2 and P_{mw}=200 mW.
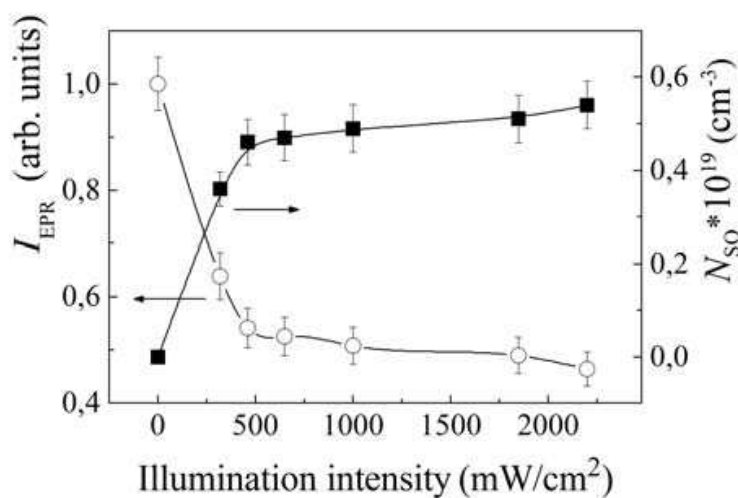

Fig. 6. Amplitude of the EPR spectra of micro-PS and the concentration of photosensitized $^1O_2$ molecules vs. I_{exc} measured at P_{mw} =200 mW and p_{O_2} =1 bar.

magnetic field to its equilibrium thermal value M_0, this quantity is also referred to as the longitudinal relaxation time. The relaxation time T_2 characterizes the relaxation of the transverse magnetization component to zero, which does not affect the total Zeeman energy

of spins but determines the width of the EPR line. The relaxation times T_1 and T_2 can be represented by the following relationships (Carrington & McLachlan, 1979):

$$\left.\begin{aligned}\frac{1}{T_1} &= \gamma^2 \left[\overline{H_x^{*2}} + \overline{H_y^{*2}} \right] \frac{\tau_c}{1 + \omega_0^2 \tau_c^2}, \\ \frac{1}{T_2} &= \gamma^2 \left[\tau_c \overline{H_z^{*2}} + \frac{1}{2} \left(\overline{H_x^{*2}} + \overline{H_y^{*2}} \right) \frac{\tau_c}{1 + \omega_0^2 \tau_c^2} \right], \end{aligned}\right\} \qquad (10)$$

where H_x^*, H_y^*, H_z^* are the components of the fluctuating magnetic field $H^*(t)$. The field $H^*(t)$ disturbs the regular spin precession in the constant field and is responsible for the exponential decay of the components of the spin vector S with the times T_1 and T_2. It is assumed that the field $H^*(t)$ is characterized by zero mean value and fluctuates with the characteristic correlation time τ_c (Carrington & McLachlan, 1979). The analysis of the system of equations (10) demonstrates that the relaxation times are related by the expression

$$\frac{1}{T_2} = \frac{1}{T_2'} + \frac{1}{2T_1} . \qquad (11)$$

In expression (11), $\dfrac{1}{T_2}$ is the EPR line width (in the absence of saturation by microwave radiation), which characterizes the homogeneous broadening of the Zeeman energy levels. This broadening is associated with the two factors: the lifetime T_1 of the spin in the excited state (the contribution $\dfrac{1}{2T_1}$) and the time characterizing the interactions that broaden the EPR line but do not lead to the spin flip, because they depend only on the fluctuating magnetic field component parallel to the constant magnetic field H_0. In our case, the fluctuating magnetic field $H^*(t)$ is governed by the anisotropy of the g factor of the spin center in PS and fluctuations of the dipole moment of the triplet oxygen molecules physically sorbed on the surface of nc-Si. In the former case, the interaction of the P_b centers with phonons through the spin–orbit interaction can be represented as the interaction of the spin center with a randomly varying magnetic field. This type of relaxation dominates in vacuum. In the presence of triplet oxygen molecules at the nanocrystal surface in the vicinity of the P_b center, the mechanism of magnetic dipole–dipole interaction between the spins of the P_b center and the $^3O_2$ molecule dominates. As a result, the P_b centers appear to be in the magnetic field induced by the oscillating magnetic moment of the physically sorbed $^3O_2$ molecules. It is this type of relaxation that dominates in the oxygen-containing atmosphere and is responsible for the increase in the amplitude of the EPR spectrum in the oxygen atmosphere as compared to vacuum (Fig. 1b). In this case, the lifetime T_1 of the P_b center in the excited state and, hence, the relaxation time T_2 should decrease in the oxygen atmosphere (see expression (11)). Actually, the analysis of the experimental data obtained by the pulsed EPR technique indicates the presence of this tendency. Figure 7 depicts the relaxation curves for the longitudinal (Fig. 7a) and transverse (Fig. 7b) components of the net magnetization of the micro-PS samples with the characteristic time T_1 and T_2, respectively.
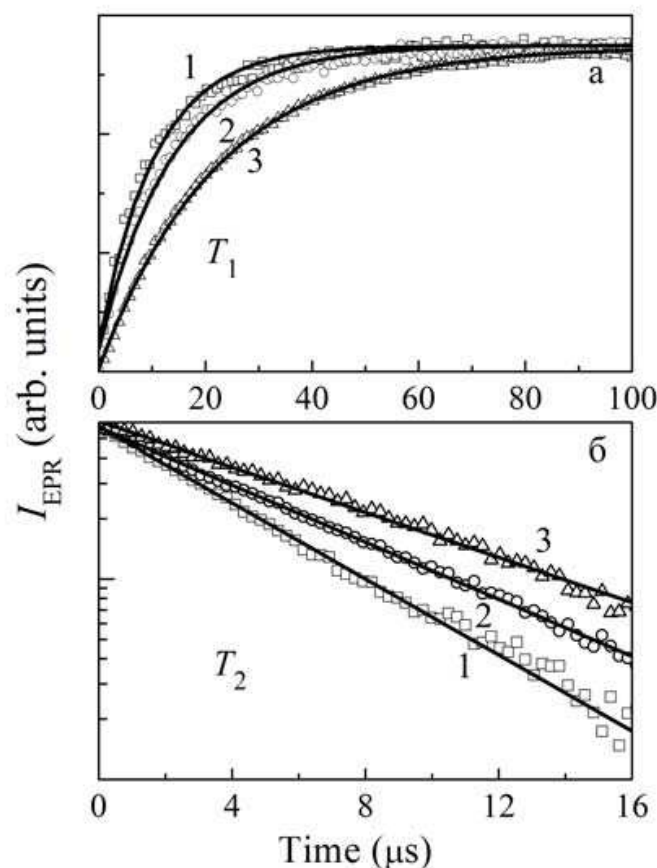
Fig. 7. Kinetics of relaxation of the (a) longitudinal and (b) transverse components of the net magnetization for the micro-PS sample in oxygen (p_{O_2} = 1 bar): (1) in the dark, (2) under illumination, and (3) in vacuum (p_{O_2} = 10⁻⁶ mbar). The experimental points are approximated by exponential functions.

It should be noted that, for PS, the net magnetization of the sample is the sum of the contributions from the spin moments of all P_b centers. With the aim of determining the relaxation times, the experimental curves were approximated by the dependences $M_0 \cdot \left(1 - 2\exp(-\frac{t}{T_1})\right)$ and $M_0 \cdot \exp(-\frac{t}{T_2})$, which made it possible to derive the relaxation times T_1 and T_2, respectively. The error in the measurements was equal to 5–7%. The paramagnetic relaxation times thus obtained for micro-PS are listed in Table 1. It can be seen from this table that the illumination of the micro-PS samples in oxygen leads to an increase in the relaxation time T_1 and, correspondingly, in the relaxation time T_2. The observed increase in the relaxation times of spin centers suggests that a number of oxygen molecules transform from the paramagnetic triplet state (participating in the dipole–dipole spin relaxation process) into the diamagnetic singlet state upon photosensitization of oxygen on the surface of nc-Si. Therefore, the pulsed EPR data confirm the generation of ¹O₂ molecules upon photoexcitation of nanocrystals in micro-PS layers. Within the limits of experimental error, the illumination of the meso-PS samples in oxygen is not accompanied by a variation in the relaxation times of spin centers (Table 1). This indicates the absence of generation of singlet oxygen in meso-PS and agrees with the data obtained by the EPR technique under

continuous microwave irradiation (see Section 3.1). Apart from the micro-PS and meso-PS samples, the Si samples were also investigated for comparison by the pulsed EPR technique. The relaxation times T_1 determined for these samples in measurements in vacuum are given in Table 1. It should be noted that the relaxation times T_1 for c-Si are in agreement with those available in the literature (Lepine, 1972). For the nc-Si, the relaxation times T_1 were determined for the first time. The analysis of the relaxation times T_1 for all the samples under investigation permitted us to reveal the following tendency: the spin–lattice relaxation process in micro-PS is retarded as compared to that in meso-PS and c-Si. In turn, the relaxation times T_1 for meso-PS are longer than those for c-Si (Table 1).

		In vacuum	In oxygen in the dark	In oxygen under illumination
Microporous silicon	T_1	22.4 ± 1.6	10.5 ± 0.7	13.8 ± 1.0
	T_2	7.7 ± 0.5	4.6 ± 0.3	6.1 ± 0.4
Mesoporous silicon	T_1	17.2 ± 1.2	11.1 ± 0.8	11.4 ± 0.8
	T_2	4.3 ± 0.3	3.4 ± 0.2	3.4 ± 0.2
c-Si	T_1	4.5 ± 0.3		

Table 1. Relaxation times of spin centers (in microseconds) at the surface of the studied samples in vacuum and in oxygen.

The retardation of the spin–lattice relaxation with a decrease in the size of the structure can be associated with the decrease in the efficiency of the electron–phonon interaction in silicon nanocrystals as compared to the bulk phase of the material under investigation. Indeed, as the size of the object decreases, the phonon spectrum undergoes substantial changes, including a partial degeneracy of phonon modes (Roodenko et al., 2010). In turn, this affects the character of the interaction between electrons and phonons that are confined in nanostructures and, in particular, leads to a decrease in the efficiency of energy transfer from excited spins to the lattice.

3.3 EPR spectroscopy of molecular oxygen

The EPR spectra of $^3O_2$ molecules in pores of micro-PS are shown in Fig. 8. It should be noted that the investigation of triplet oxygen by the EPR technique was performed in the millimeter (Q) band of microwave radiation in view of a large width (approximately 10 kG) of the EPR spectrum of $^3O_2$ molecules (due to the short lifetime in the excited state (Vahtras et al., 2002)). The presence of several lines in the EPR spectrum (Fig. 8) is determined by the strong interaction of the rotational angular momentum K and the spin angular momentum S of the oxygen molecule.

The total angular momentum J takes on values K and K ± 1 (because S = 1). As a rule, the recorded EPR spectrum contains six lines designated as C, E, F, G, K, and J, which have the
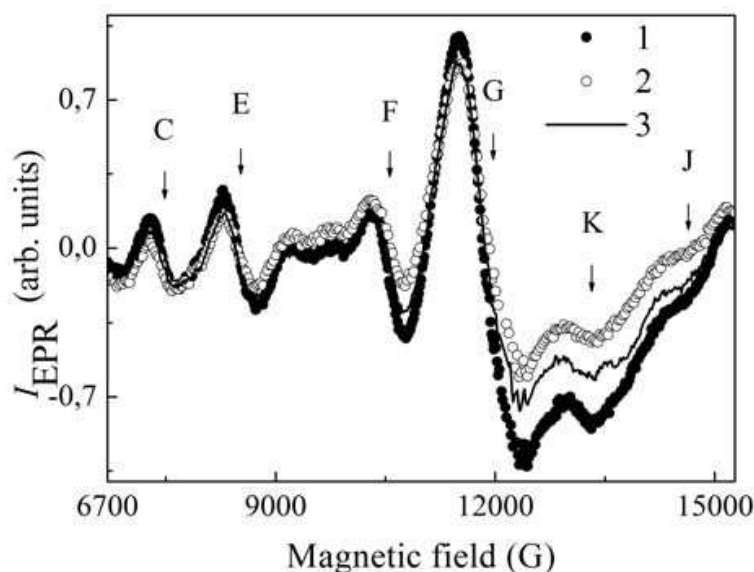
Fig. 8. EPR spectra of molecular oxygen in layers of micro-PS: (1) in the dark, (2) under illumination, and (3) within 5 min after the cessation of illumination. Experimental conditions: P_{mw} =200 mW, I_{exc}=650 mW/cm², and p_{O_2} =0.5 bar.

highest intensities (Vahtras et al., 2002). They correspond to the following magnetic dipole transitions J, $M_J \rightarrow J/$, $M_J/$: {1, -1 → 1, 0} (C); {2, 1 → 2, 2} (E); {2, 0 → 2, 1} (F); {6, -2 → 4, -1} (G); {2, -1 → 2, 0} (K) and {2, 1 → 2, 2} (J). It can be seen from Fig. 8 that the illumination of the samples results in a decrease in the amplitude of the EPR spectrum. This suggests a decrease in the concentration of triplet oxygen molecules. The data obtained can be explained by the transition of oxygen molecules to the singlet state and can be considered a direct proof of the generation of $^1O_2$ molecules in micro-PS layers. It should be noted that the EPR signal amplitude after the illumination is switched off only partially regains its initial value (before illumination) (Fig. 8). This can be explained by the fact that a considerable number of $^1O_2$ molecules pass from pores of the sample into the closed volume of the measuring cell, i.e., into the gaseous medium, in which the lifetime of the singlet state increases to approximately 50 min as compared to approximately 500 μs in pores of silicon (Gross et al., 2003). Since the area under the EPR line is proportional to the number of spin centers, it is easy to estimate the fraction of the newly formed singlet oxygen molecules from the relationship $\alpha = 1 - \dfrac{S_{light}}{S_{dark}}$, where S_{light} and S_{dark} are the areas under the EPR lines of $^3O_2$ molecules under illumination and in the dark, respectively. Therefore, approximately 30% of oxygen molecules upon photoexcitation of nanocrystals in micro-PS layers transform into the singlet state. It should be noted that similar experiments with meso-PS revealed no changes in the amplitude of the EPR spectrum of triplet oxygen molecules in pores of mesoPS. This indicates that $^1O_2$ molecules are not formed in this material (see Sections 3.1, 3.2).

3.4 Kinetic equations for the relaxation processes in nc-Si ensembles

We now develop kinetic equations for an ensemble of excited nanocrystals in PS samples in vacuum. To his end, we consider a model fragment of the PS microstructure, namely, a

chain of spherical nc-Si crystals having a diameter changing in small limits and forming a quantum filament of a variable cross section (Fig. 9a). This model representation agrees with the real structure of micro-PS, whose layers consist of nc-Si crystals no more 5 nm in size. Figure 9 shows micrographs of micro-PS films produced by the anodic oxidation of p-type silicon wafers. They clearly exhibit nc-Si chains forming silicon filaments of a variable cross section (Cullis & Canham, 1991). We number neighboring nanocrystals in a chain beginning from a zeroth crystal with the maximum size as 0, …, m – 1, m, m + 1, …, M, where m = 0, 1, 2, …, M. In the case of a fractal PS model (Moretti et al., 2007; Nychyporuk et al., 2005), m has the meaning of an ordinal number that is repeated when the nanofragment (nanocrystal) scale decreases, $d_m = d_0 k^{-m}$, where k > 1 is the linear scale reduction coefficient and d_0 is he diameter of the largest crystal. Let N_m be the number of nc-Si crystals with ordinal number m; then, N_m can be written as $N_m = N_{0m} + N_{1m} + N_{2m}$, where N_{0m}, N_{1m}, and N_{2m} are the numbers of unexcited nc-Si crystals and nc-Si crystals containing one and two excitons, respectively. The number of nc-Si crystals with more than two excitons is negligibly small as compared to N_{2m} because of the rapid Auger recombination processes that occur when the number of excitons in a nanocrystal is larger than one.
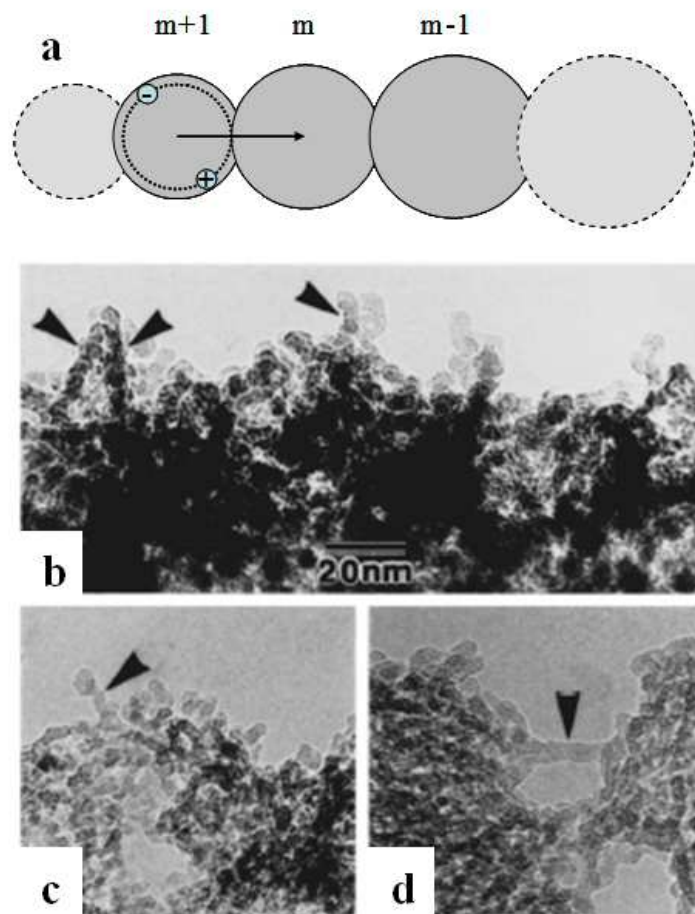

Fig. 9. (a) Model for a fragment of one of the quantum filaments of a variable cross section that form the PS microstructure and (b–d) transmission electron microscopy micrographs of PS layers (Cullis & Canham, 1991). The arrows indicate columnar structures.

Moreover, N_m' is the number of nc-Si crystals with point defects (no less than one per crystal; N_m' is part of the total number of nc-Si crystals N_m). In general, all primed quantities relate to the processes that take place in nc-Si crystals with defects. Then, a set of kinetic equations describing the energy relaxation for N_{0m}, N_{1m}, and N_{2m} after the end of optical excitation is (point above a quantity means differentiation with respect to time t)

$$\left.\begin{array}{l} \dot{N}_{1m} = -\alpha_{rm}N_{1m} - \alpha_m'N_{1m}' - D_m N_{1m}N_{0m-1} - D_m^* N_{1m}N_{1m-1} + D_{m+1}N_{1m+1}N_{0m} - D_{m+1}^* N_{1m+1}N_{1m}, \\ \dot{N}_{0m} = \alpha_{rm}N_{1m} + \alpha_m'N_{1m}' + D_m N_{1m}N_{0m-1} + D_m^* N_{1m}N_{1m-1} - D_{m+1}N_{1m+1}N_{0m} + \alpha_A N_{2m}, \\ \dot{N}_{2m} = -\alpha_{Am}N_{2m} + D_{m+1}^* N_{1m+1}N_{1m}. \end{array}\right\} \quad (12)$$

The meaning of the parameters entering into the set of nonlinear differential equations (12) is as follows: α_{rm} and α_m' are the rates of radiative and nonradiative recombination, respectively. Obviously, the latter takes place only in nc-Si with defects. The dimension of the α coefficients is µs^{-1}. D_m and D_m^* are the coefficients of exciton migration from nc-Si with ordinal number m to nc-Si with ordinal number m–1, i.e., toward larger nanocrystals (toward a decrease in the energy gap due to the quantum size effect; Fig. 9a). D_m^* describes the efficiency of exciton migration into a nanocrystal having an exciton before the transfer event. Since the dimension of coefficient D is cm^3 µs^{-1}, it can be formally interpreted as the product of the translational thermal exciton velocity into the transfer cross section. Finally, α_{Am} is the Auger recombination rate (µs^{-1}). In total, all three equations of set (12) yield zero, since

$$\frac{dN_{0m}}{dt} + \frac{dN_{1m}}{dt} + \frac{dN_{2m}}{dt} = \frac{dN_m}{dt} = 0$$

Let us explain the physical meaning of the terms of type $D_m N_{1m}N_{0m-1}$. This term describes the exciton migration from nc-Si with concentration N_{1m} (i.e., from nc-Si crystals having ordinal number m and containing one exciton) to nc-Si with concentration N_{0m-1} (neighboring unexcited larger nc-Si crystals). In the third equation of the set for nc-Si crystals with concentration N_{2m}, we neglected the terms responsible for the exciton migration from these nanocrystals ($-D_m N_{2m}N_{0m-1} - D_m^* N_{2m}N_{1m-1}$) and radiative recombination ($-\alpha_{rm}N_{2m}$) assuming that the Auger recombination is a much faster process. Indeed, α_{Am} for nc-Si is 10^{-8} –10^{-9} s (Proot et al., 1992; Delerue et al., 1993), whereas the characteristic migration and radiative recombination times fall in the microsecond range, as follows from an analysis of the experimental PL relaxation kinetics (see below). Moreover, in the third equation of set (12), we neglected the terms of type $-\alpha_m'N_{2m}'$, which describe nonradiative recombination at defects in nc-Si crystals with two excitons. This assumption is reasonable, since the probability of the presence of two excitons in one nc-Si crystal with a defect is negligibly low. Indeed, an exciton in an nc-Si crystal with a defect undergoes nonradiative annihilation before the transfer of another exciton in this nc-Si crystal at a high probability, since the time of carrier trapping by a neutral defect (10^{-9} –10^{-11} s) for the nanocrystals that luminesce in the red spectral region (which have an energy gap 1.3 < Eg < 2.2 eV) is extremely short (Delerue et al., 1993). If we consider the case of nanocrystals that do not luminesce in this spectral region (for which α' is comparable with the radiative recombination rate (Delerue

et al., 1993), $\alpha'_m N'_{2m}$ term and the terms describing radiative recombination and the exciton migration from these nc-Si crystals may be neglected due to their smallness compared to term $\alpha_{Am} N_{2m}$ (Delerue et al., 1993). We now consider the kinetic equation that describes the nonradiative recombination of excitons in nc-Si crystals with defects,

$$\dot{N}'_{1m} = -\alpha' N'_{1m} - \alpha_{rm} N'_{1m} - D_m N'_{1m} N_{0m-1} - D^*_m N'_{1m} N_{1m-1} - D^*_{m+1} N_{1m+1} N'_{1m} + D_{m+1} N_{1m+1} N'_{0m} \qquad (13)$$

We substitute $(N'_m - N'_{1m})$ for N'_{0m}, group the terms, and obtain the expression

$$\dot{N}'_{1m} = -\left[\alpha'_m + \alpha_{rm} + D_m N_{0m-1} + D^*_m N_{1m-1} + (D^*_{m+1} + D_{m+1}) N_{1m+1} \right] N'_{1m} + D_{m+1} N_{1m+1} N'_m \qquad (14)$$

We analyze this expression by analogy with the procedure performed for $\dot{N}_{2m}$ and conclude that all terms in the square brackets may be neglected compared to α'_m. Below, we will prove the legitimacy of these assumptions for luminescent nc-Si crystals. Allowing for these assumptions, we write kinetic equations for nc-Si crystals in which rapid relaxation processes take place:

$$\left. \begin{array}{l} \dot{N}'_{1m} = -\alpha'_m N'_{1m} + D_{m+1} N_{1m+1} N'_m, \\ \dot{N}_{2m} = -\alpha_{Am} N_{2m} + D^*_{m+1} N_{1m+1} N_{1m}. \end{array} \right\} \qquad (15)$$

Let us analyze the processes that occur in such nc-Si crystals immediately after removing an optical excitation in detail. If the initial values of N'_{1m} and N_{2m} are sufficiently high, they decrease rapidly in 10^{-6} –10^{-9} s via nonradiative and Auger recombination (Delerue et al., 1993). Beginning from the time when the recombination rates become equal to the rate of filling of these nanocrystals due to the exciton migration from nc-Si crystals with larger ordinal numbers, these processes manifest themselves as negative-feedback systems to some extent. For example, if the inequality $\alpha'_m N'_{1m} > D_{m+1} N_{1m+1} N'_m$ holds true at a certain time, concentration N'_{1m} decreases ($\dot{N}'_{1m} < 0$). As a result, the absolute value of the rate of loss of excitons N'_{1m} (which is proportional to $\alpha'_m N'_{1m}$) decreases and $D_{m+1} N_{1m+1} N'_m$ remains constant (since it is independent of N'_{1m}). Finally, the rates of loss and supply of excitons in nc-Si crystals become the same and the equality $\dot{N}'_{1m} = 0$ again takes place. Similarly, if $\dot{N}'_{1m} > 0$, rate $\alpha'_m N'_{1m}$ increases in absolute value and again becomes equal to the rate of exciton supply to the ensemble of nc-Si crystals due to migration from neighboring nanocrystals. The same is true for the number of nc-Si crystals with two excitons (N_{2m}). Thus, the approximate equalities

$$\left. \begin{array}{l} \dot{N}'_{1m} \approx 0, \\ \dot{N}_{2m} \approx 0. \end{array} \right\} \qquad (16)$$

hold true due to the substantial difference in the rates of rapid recombination processes and slow migration processes at any time beginning from approximately 10^{-6} s after removing an optical excitation. With the first equation from set (16), we can express N'_{1m} and substitute it into the first equation of set (12), and the second equation of set (16) demonstrates that $N_{2m} \ll N_{1m}$. Indeed, we have

$$N_{2m} = \left(\frac{D^*_{m+1} N_{1m+1}}{\alpha_{Am}} \right) N_{1m} << N_{1m}. \tag{17}$$

Based on inequality (17), we neglect N_{2m} compared to N_{1m} in an expression for the number of unexcited nc-Si crystals:

$$N_{0m} = N_m - N_{1m} - \cancel{N}_{2m}.$$

As a result of this simplification, the substitution of N'_{1m}, and the regrouping of the terms, we reduce the first equation of set (12) to the form

$$\dot{N}_{1m} = -\alpha_{rm} N_{1m} - D_m N_{1m} N_{m-1} + (D_m - D^*_m) N_{1m} N_{1m-1} - \\ -(D_{m+1} + D^*_{m+1}) N_{1m+1} N_{1m} + D_{m+1} N_{1m+1} (N_m - N'_m) \tag{18}$$

Although set (12) is substantially simplified, it is rather difficult to directly solve Eq. (18) even using numerical methods. First, the total number of equations can be rather large, since m varies from zero to M. The value of parameter M can easily be estimated in a fractal model, since it represents the order of the minimum size nc-Si crystal with a diameter $d_M = d_0 k^{-M}$. For estimation, we assume $d_M = 0.6$ nm (which is the double Si–Si bond length) and $d_0 = 5$ nm (see Figs. 9b–1d) and obtain

$$M = \frac{\ln(d_0 / d_M)}{\ln k} \approx \frac{2.1}{\ln k}.$$

Thus, M depends on coefficient k of linear scale reduction, which can be only insignificantly higher than unity in the case of crystals having almost the same sizes; as a result, M can be arbitrarily large. For example, at k = 1.02 we have M = 107. Second, the character of the dependence of recombination rate α and, especially, migration coefficient D on ordinal number m is unknown. Thus, to solve the set of equations (18), we have to know the dependences of these parameters on the nc-Si crystal size over the entire size range (in our case, from 0.6 to 5 nm). Nevertheless, equations (18) become much simpler if we assume "local quasi-identity" of nc-Si crystals, i.e., if we assume that neighboring nc-Si crystals with numbers m–1, m, and m+1 and several farther neighbors have similar shapes and sizes. The larger the number of almost identical nc-Si crystals in a chain, the more adequate this assumption. In a fractal model of the structure of PS, this assumption means that k is close to unity. Then, the number of neighbors of any nc-Si crystal is $n = k^{D_F}$, where D_F is the fractal dimension of nc-Si (which ranges from 2.2 to 2.6) (Nychyporuk et al., 2005). Taking $D_F = 2.4$ and $k = 1.02$, we obtain $n \approx 1.05$. The structure described by these values of parameters n and k is represented by long filaments made of almost the same nc-Si crystals (the difference in the neighboring crystal sizes is approximately 2%) intersecting with other filaments every 20 nc-Si crystals. As follows from Figs. 9b–9d, this structural model is close to reality. With the assumption of local quasi-identity of nc-Si crystals, we can omit all ordinal indices in Eq. (18) assuming that

$$\begin{aligned} N_{m-1} &\approx N_m \approx N_{m+1} \equiv N, \\ N_{1m-1} &\approx N_{1m} \approx N_{1m+1} \equiv N_1, \\ D_{m-1} &\approx D_m \approx D_{m+1} \equiv D, \\ \alpha_{rm-1} &\approx \alpha_{rm} \approx \alpha_{rm+1} \equiv \alpha_r, \end{aligned} \tag{19}$$

and so on. As a result, we can rewrite Eq. (18) in the form

$$\dot{N}_1 = -\alpha_r N_1 - DN_1 N + (D - D^*)N_1^2 - (D + D^*)N_1^2 + DN_1(N - N') \tag{20}$$

and eventually obtain the following kinetic equation for the relaxation of an optical excitation in an ensemble of nc-Si crystals with allowance for exciton transfer in them:

$$\dot{N}_1 = -\alpha N_1 - 2D^* N_1^2, \\ \alpha \equiv \alpha_r + DN', \tag{21}$$

where we introduced a designation for the sum $\alpha_r + DN'$. Note that term $-2D^* N_1^2$ in Eq. (21), which causes a nonexponential decrease in the PL intensity, depends only on the migration coefficient, which describes the exciton transfer to an excited neighboring crystal (which contains an exciton before the transfer event). Thus, it is ultrafast Auger recombination processes that determine the nonexponential relaxation of an ensemble of coupled nc-Si crystals. Note that the values of coefficients D and D^* should be close. The small difference between them can be caused by an additional interaction of excitons located in neighboring nc-Si crystals (in the case of D^*). In the dipole approximation, we have $D=D^*$, since the trace of the symmetric dipole–dipole interaction tensor is zero (Carrington & McLachlan, 1979). Therefore, the energy of this interaction is also zero upon averaging over a spherically symmetric exciton charge distribution. The difference in coefficients D and D^* can be related to the presence of a quadrupole (or higher moments of) interaction of excitons or an exchange interaction in the case of a substantial overlapping of their wavefunctions. Obtained ordinary differential equation (21) is a Bernoulli equation with constant coefficients and an exponent γ=2 of the highest degree of the unknown function. This equation is solved analytically using the substitution $y = N_1^{1-\gamma} = 1/N_1$. With allowance for the initial condition $N_1(t = 0) = N_1^{(0)}$, the solution to Eq. (21) has the form

$$N_1(t) = \frac{\alpha N_1^{(0)}}{\alpha \exp(\alpha t) + 2D^* N_1^{(0)}(\exp(\alpha t) - 1)}. \tag{22}$$

Obviously, the product $\alpha_r N_1(t)$ describes the PL intensity decrease kinetics for an ensemble of nc-Si crystals of a given size. Let us note some advantages of Eq. (22) over stretched exponent (1). The absence of migration ($D = D^* = 0$) leads to the usual monoexponential character of a decrease in the PL intensity with increasing radiative lifetime, according to the experimental kinetics obtained for nc-Si crystals separated by a thick oxide SiO$_2$ layer (Vinciguerra et al., 2000). The form of the normalized kinetics $\frac{\alpha_r N_1(t)}{N_1^{(0)}}$ depends on $N_1^{(0)}$ excitation level, which was repeatedly noted by many researchers (see, e.g., (Chen et al., 1992)). At $t \rightarrow \infty$, the $N_1(t)$ curve has a monoexponential drop, which agrees well with the experimental data (see below). Defect concentration N' contributes substantially (in the product with D; see Eq. (21)) to optical excitation relaxation rate α, in contrast to the case without migration. If excitons did not move along an nc-Si network ($D = D^* = 0$), the normalized PL intensity decrease kinetics would not depend on the defect concentration,

which is in conflict with the experimental data (see below). Thus, energy transfer via exciton migration does occur in an ensemble of coupled nc-Si crystals. Note that, if we do not neglect terms α_{rm} and $D_m N_{m-1}$ compared to α'_m in Eq. (14), we can obtain a more accurate expression $\alpha \equiv \alpha_{acc}$,

$$\alpha_{acc} = \alpha_r + \frac{\alpha'}{\alpha' + \alpha_r + DN} DN'. \tag{23}$$

However, a numerical analysis with the Mathcad software package demonstrates that the factor multiplying DN' in Eq. (23) differs from unity by several fractions of a percent for luminescent silicon nanocrystals. The experimental PL relaxation curves of micro-PS samples can be approximated by analytical dependence (22) using α and $\zeta = 2D^* N_1^{(0)}$ as fitting parameters. The results of this process will be presented below. It is interesting to find the value of diffusion coefficient D^* using the well-known value of approximation parameter ζ. To this end, we have to determine $N_1^{(0)}$ initial excitation level. As will be shown in the next section, such a calculation can be performed in terms of the proposed model.

3.5 Photoluminescence of porous silicon under steady-state photoexcitation conditions

We write the first and second equations from set (12) for a steady-state case ($\frac{d}{dt} = 0$) in the presence of an optical excitation in the system $g_m \left[\mu s^{-1} \right] = \sigma_m I_{ex}$ (where σ_m is the absorption cross section of nanocrystals with ordinal number m (i.e., nanocrystals of a certain size; see Section 3.4) and I_{ex} is the radiation intensity):

$$\left. \begin{array}{l} \dot{N}_{1m} = g_m N_{0m} - \alpha_{rm} N_{1m} - \alpha'_m N'_{1m} - D_m N_{1m} N_{0m-1} - D^*_m N_{1m} N_{1m-1} + \\ \quad + D_{m+1} N_{1m+1} N_{0m} - D^*_{m+1} N_{1m+1} N_{1m} = 0, \\ \dot{N}_{2m} = g_m N_{1m} + D^*_{m+1} N_{1m+1} N_{1m} - \alpha_{Am} N_{2m} = 0. \end{array} \right\} \tag{24}$$

Note that an analysis of the last equation in set (24) immediately yields the inequality $N_{2m} \ll N_{1m}$; whence, it also follows that $N'_{2m} \ll N'_{1m}$. Indeed, the equality

$$\frac{N'_{2m}}{N_{2m}} = \frac{N'_{1m}}{N_{1m}} = \frac{N'_m}{N_m}$$

is obvious in the steady-state case. It reflects the fact that these relations are determined by the fraction of defect-containing nc-Si crystals of the total number of nc-Si crystals in the same manner. Based on the inequalities, we may neglect N_{2m} and N'_{2m} in the following expressions:

$$N_{0m} = N_m - N_{1m} - \cancel{N_{2m}} \text{ and } N'_{0m} = N'_m - N'_{1m} - \cancel{N'_{2m}}$$

We substitute the latter expression into the equation for nc-Si crystals with defects, which is analogous to the first equation in set (24) in which N_{0m} and N_{1m} substitute for N'_{0m} and N'_{1m}, and have

$$N'_{1m} = \frac{(g_m + D_{m+1}N_{1m+1})N'_m}{g_m + \alpha_{rm} + \alpha'_m + D_m N_{m-1} - (D_m - D^*_m)N_{1m-1} + (D_{m+1} + D^*_{m+1})N_{1m+1}}. \tag{25}$$

Based on the causes described in the previous section, we neglect all quantities in the denominator as compared to α'_m in the last expression and substitute it in the first equation in set (24). We now group the terms, take into account the consideration about the smallness of N_{2m} given above, and write the first equation of set (24) in the form

$$0 = g_m(N_m - N'_m) - N_{1m}(g_m + \alpha_{rm} + D_m N_{m-1}) + (D_m - D^*_m)N_{1m-1}N_{1m} + \\ + D_{m+1}N_{1m+1}(N_m - N'_m) - (D_{m+1} + D^*_{m+1})N_{1m+1}N_{1m} \tag{26}$$

This is the general form of an equation for the number of photoexcited nc-Si crystals of the mth order in a fractal chain in the steady-state case. This equation can be solved by an iteration method beginning from $m = 0$. However, this process is related to the difficulties described in the previous section. At the same time, Eq. (26) can be solved in the local nc-Si quasi-identity approximation, which is represented by Eqs. (19). As a result, we obtain the following quadratic equation for N_1, in which ordinal indices are omitted:

$$2D^* N_1^2 + \alpha_{ex} N_1 - g(N - N') = 0, \\ \alpha_{ex} \equiv g + \alpha = g + \alpha_r + DN', \tag{27}$$

where we introduced a designation for $g + \alpha_r + DN'$ similarly to Eq. (21). The nonnegative solution to Eq. (27) has the form

$$N_1^{(0)} = \sqrt{\left(\frac{\alpha_{ex}}{4D^*}\right)^2 + \frac{g(N - N')}{2D^*}} - \frac{\alpha_{ex}}{4D^*}. \tag{28}$$

Note that a more accurate (by several fractions of a percent) solution can be obtained if we do not neglect $g_m + \alpha_{rm} + D_m N_{m-1}$ as compared to α'_m in Eq. (25). In this case, N' in Eq. (28) is everywhere replaced by the product

$$\varepsilon' N' \equiv \frac{\alpha'}{g + \alpha' + \alpha_r + DN} N',$$

in which correcting coefficient ε' is insignificantly smaller than unity for relatively low optical excitation levels as compared to the significant rate of nonradiative recombination at a defect α' for luminescent nc-Si crystals.

In the limiting case $D^* = 0$, Eq. (28) is reduced to the form

$$N_1^{(0)}\Big|_{D^*=0} = \frac{g(N - N')}{g + \alpha_r}, \tag{29}$$

that is, it coincides with the solution to set (24) in the absence of the terms describing migration. According to Eq. (29), steady-state PL intensity of nc-Si ensembles $I_{PL} \propto N_1^{(0)}$ weakly depends on the defect concentration in them, since the fraction of defect-containing nc-Si crystals of the total number of nc-Si crystals ($\frac{N'}{N}$) is low (10^{-3} –10^{-2}). However,

according to the experimental data, the PL spectrum amplitude decreases significantly during the photostimulated oxidation of PS samples (see below), whereas the defect concentration increases only by a factor of 1.5–2 (see below). Therefore, as in the case of the kinetic curves of PL decay (Section 3.4), the motion of excitons along a network of coupled nc-Si crystals also substantially affects the steady-state PL intensity. To express diffusion coefficient D^* through parameters α_{ex} and ζ, we multiply both sides of Eq. (28) by $2D^*$

$$\zeta \equiv 2D^* N_1^{(0)} = \sqrt{\left(\frac{\alpha_{ex}}{2}\right)^2 + 2D^* g(N - N')} - \frac{\alpha_{ex}}{2}, \tag{30}$$

as a result, we have

$$D^* = \frac{\zeta(\alpha_{ex} + \zeta)}{2g(N - N')} \approx \frac{\zeta(\alpha_{ex} + \zeta)}{2gN}, \tag{31}$$

where we neglected N' compared to N in the last equality (see above). Thus, the exciton migration coefficient averaged over the entire ensemble of nc-Si crystals of a given size can be calculated by Eq. (31) using approximation parameters α and ζ of the kinetic dependences of PL decay and determining photoexcitation level g and the nc-Si concentration in the ensemble. Although the latter is most difficult, it can be performed in terms of a fractal PS model. Indeed, the number of nc-Si crystals of a given size (in this case, about 3 nm, which corresponds to an energy gap of 1.6 eV (Delerue et al., 1993)) can readily be estimated from the following expression for the number of nc-Si crystals of order m: $N_m = N_0 k^{D_F m}$, where N_0 is the number of nc-Si crystals of the zeroth order, $k=1.02$ is the linear scale reduction coefficient (according to the local quasi-identity approximation; see Section 3.4), $D_F=2.4$ is the fractal dimension of PS layers, and m ranges from zero to $M = 107$ (see Section 3.4). The total number of nc-Si crystals of all orders is

$$N_{\text{tot}} = \sum_{m=0}^{M} N_m = \frac{k^{MDF} - 1}{k^{DF} - 1} N_0 \approx 3300 N_0.$$

We assume that $N_{tot}=10^{21}$ cm^{-3} and determine N_0. The order corresponding to an nc-Si diameter $d_m=3$ nm is expressed as

$$m = \frac{\ln(d_0 / d_m)}{\ln k} = \frac{\ln(5 / 3)}{\ln 1.02} \approx 26,$$

as a result, we obtain

$$N_{26} = \frac{N_{\text{tot}}}{3300} 1.02^{2.4 \cdot 26} \approx 10^{18} cm^{-3}.$$

Similarly, knowing the total number of nc-Si crystals with defects (about 10^{17} cm^{-3}) or oxygen molecules (at p_{O_2} =1 bar, n=2.4·10^{19} cm^{-3}) and taking into account that their specific number per nanocrystal is proportional to the nanocrystal surface area, we can estimate the number of defects (about 10^{15} cm^{-3}) or O_2 molecules (about 2·10^{17} cm^{-3}) per ensemble of nc-Si crystals of a given size (with an ordinal number $m=26$). At a nitrogen laser radiation

intensity of 300 mW/cm^2 and an quantum energy of 3.7 eV, I_{ex} = 5·10^{17} photons/(cm^2 s) are incident on a sample. Assuming that the absorption cross section of a PS sample is σ=10^{-14} cm^2 (Bisi et al., 2000), we find that the optical photoexcitation rate is $g = I_{ex}\sigma \approx 0.005$ μs^{-1}. Allowing for $\alpha \approx 0.008$ μs^{-1}, we obtain $\alpha_{ex} = g + \alpha \approx 0.013$ μs^{-1}. The characteristic value of α was taken from the results of approximation of the kinetic dependences for coarse-grained PS powders with a porosity P= 70% (table 2). The approximation parameter is ζ =0.038 μs^{-1} (table 2).

	PS 1 (P = 70%)		PS 2 (P = 85%)	
	CG	FG	CG	FG
α^{-1}, μs	126 ± 13	128 ± 13	117 ± 12	126 ± 13
ζ^{-1}, μs	26 ± 3	49 ± 5	104 ± 10	72 ± 7

Table 2. Parameters of the approximation of the kinetic PL decay curves shown in Fig. 15 by Eq. (22).

Substituting these values of parameters into Eq. (31), we finally obtain the migration coefficient for coarse-grained (P=70%) PS samples, D^* =3.9·10^{-13} cm^3/s. Using Eq. (28) and the values of all necessary parameters determined above, we can construct a relationship between the number of excited nc-Si crystals $N_1^{(0)}$ and, e.g., the level of optical excitation or the defect concentration (for nanocrystals with defects; see Fig.10). It is seen that, in the presence of nonradiative recombination centers, the PL of the entire ensemble ($I_{PL} = \alpha_r N_1^{(0)}$) is quenched in all nc-Si crystals, which agrees with the conclusions in (Delerue et al., 1993) (Fig. 10a). The dependences of the PL intensity of a sample in vacuum on the level of optical excitation (Fig. 10b) agree qualitatively with the experimental curves (see, e.g., (Gross et al., 2003)). Based on the developed theory, we can estimate the radiative lifetimes of the PL of an ensemble of nc-Si crystals. Indeed, when analyzing experimental kinetics, we obtain approximation parameter α, which is expressed through radiative recombination rate α_r as $\alpha \equiv \alpha_r + DN'$ (see Eq. (21)). The concentration of point defects in as-deposited micro-PS films is low, so that $DN' << \alpha_r$; therefore, we may assume $\alpha \approx \alpha_r$ for estimation.

3.6 Theoretical analysis of the singlet oxygen generation efficiency

We now consider an ensemble of nc-Si crystals of a certain size under conditions of steady-state photoexcitation in an oxygen-containing medium and still assume that the local nc-Si quasi-identity approximation holds true (see Section 3.4). Then, the condition of dynamic equilibrium between the number of O$_2$ molecules in the singlet (n_{SO}) and triplet (n_{TO}) states is

$$\left.\begin{aligned} \dot{n}_{SO} = \alpha_{ET} N_1 \frac{n_{TO}}{N} - \alpha_{SO} n_{SO} = 0, \\ n_{SO} + n_{TO} = n \end{aligned}\right\}, \tag{32}$$

where α_{ET} is the probability of energy transfer per unit time from an excited Si nanocrystal to one oxygen molecule adsorbed on its surface. The first term takes into account the fact that the interaction efficiency is proportional to the number of ^{3}O$_2$ molecules per nc-Si ($\frac{n_{TO}}{N}$).

Quantity α_{SO}^{-1} is the oxygen molecule lifetime in the singlet state in PS pores, which is about 500 µs (Gross et al., 2003), and n is the concentration of O_2 molecules. Here, for simplicity, the number of excited nc-Si crystals (N_1) is written without superscript (0), which means that a steady-state case is analyzed. Using Eq. (32), we can easily express the stationary concentration of ${}^3O_2$ molecules,

$$n_{TO} = \frac{\alpha_{SO} N n}{\alpha_{SO} N + \alpha_{ET} N_1}. \tag{33}$$

For an oxygen-containing medium, the term $\alpha_{ET} N_1 \dfrac{n_{TO}}{N}$ is added to the left-hand side of Eq. (27); this term is responsible for the energy transfer from annihilating excitons to triplet oxygen molecules on the nc-Si surface. After the substitution of Eq. (33) for n_{TO} and some manipulations, we write Eq. (27) in the form

$$2D^* \alpha_{ET} N_1^3 + \left(\alpha_{ET} \alpha_{ex} + 2D^* \alpha_{SO} N \right) N_1^2 + \\ + \left(\alpha_{ET} \alpha_{SO} n + \alpha_{ex} \alpha_{SO} N - \alpha_{ET} g(N - N') \right) N_1 - \alpha_{SO} g(N - N') N = 0. \tag{34}$$

This is a cubic equation for N_1, which can be solved numerically. We used the Mathcad software package. With Eq. (33) and the solution to Eq. (34), we obtain the following expression for the concentration of photosensitized ${}^1O_2$:

$$n_{SO} = n - n_{TO} = \frac{\alpha_{ET} N_1 n}{\alpha_{SO} N + \alpha_{ET} N_1}. \tag{35}$$

Figure 11 shows the calculated dependence of the fraction of singlet oxygen on the nc-Si photoexcitation rate at various molecular oxygen concentrations.

Hereafter, by default we use the following parameters for numerical simulation, unless otherwise specified (see Section 3.4): $D \approx D^* = 3.9 \cdot 10^{13}$ cm^3/s, $N = 10^{18}$ cm^{-3}, $N' = 10^{15}$ cm^{-3}, $\alpha_r^{-1} = 125$ µs, $\alpha_{ET}^{-1} = 40$ µs (Gross et al., 2003), and $\alpha_{SO}^{-1} = 500$ µs (Gross et al., 2003). The curves in Fig. 11 are similar to the experimental dependence of the concentration of ${}^1O_2$ molecules on the photoexcitation intensity obtained by EPR (see Fig.6). When oxygen partial pressure p_{o_2} increases, the concentration of forming ${}^1O_2$ increases (Fig. 12a); however, the fraction of O_2 molecules in the singlet state of the total number of O_2 molecules decreases beginning from a certain value of p_{o_2} (Figs. 11 and 12b). Indeed, until the number of O_2 molecules per Si nanocrystal in the ensemble under study is smaller than a certain value, the fraction of ${}^1O_2$, which is only determined by the relation between the characteristic times of excitation, relaxation, and energy transfer, remains constant with increasing pressure. When the specific number of O_2 molecules reaches a certain threshold value (more than unity) per nc-Si crystal, this crystal cannot excite all oxygen molecules adsorbed on its surface at the same efficiency. As a result, the fraction of ${}^1O_2$ decreases when the concentration of molecular oxygen increases further (Fig. 12b). The difference between the curves shown in Fig. 12a and the curve obtained experimentally by EPR (see Fig.5b) can be caused by the integral character of EPR: a microwave power signal of absorption by all spin centers (Pb-centers) in a sample is measured in this technique, whereas many of them do not interact with O_2 molecules at a low oxygen concentration and, thus, are insensitive to a change in the ${}^1O_2$ concentration.
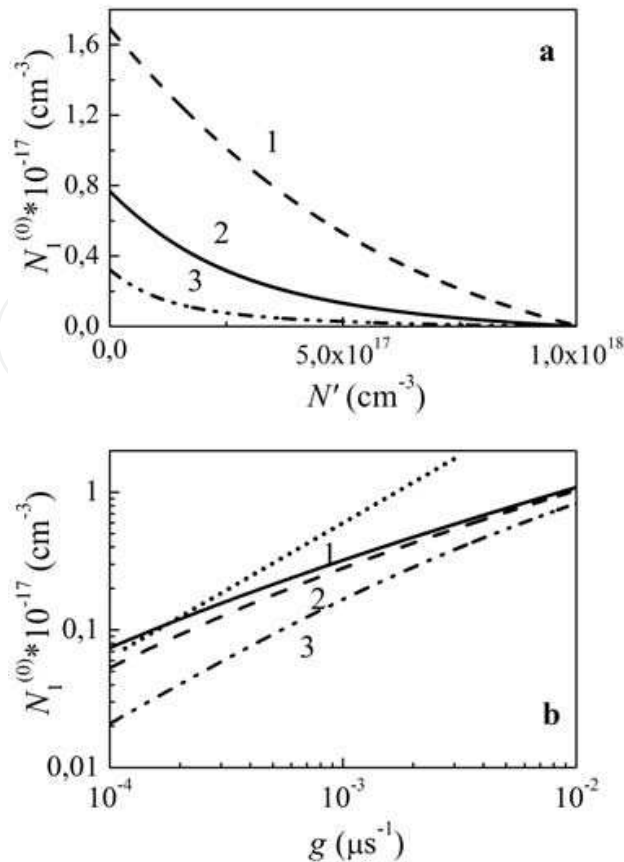
Fig. 10. Calculated dependences of the steady-state PS PL intensity in vacuum ($I_{PL} \propto N_1^{(0)}$) on (a) the concentration of nc-Si crystals with defects N' at g=(1) 0.025, (2) 0.005, and (3) 0.001 μs^{-1} and on (b) g at N'=(1) 10^{15}, (2) $2 \cdot 10^{16}$, and (3) 10^{17} cm^{-3}. The total number of nc-Si crystals in the ensemble is 10^{18} cm^{-3}. A linear dependence is shown as a dashed line for clarity.
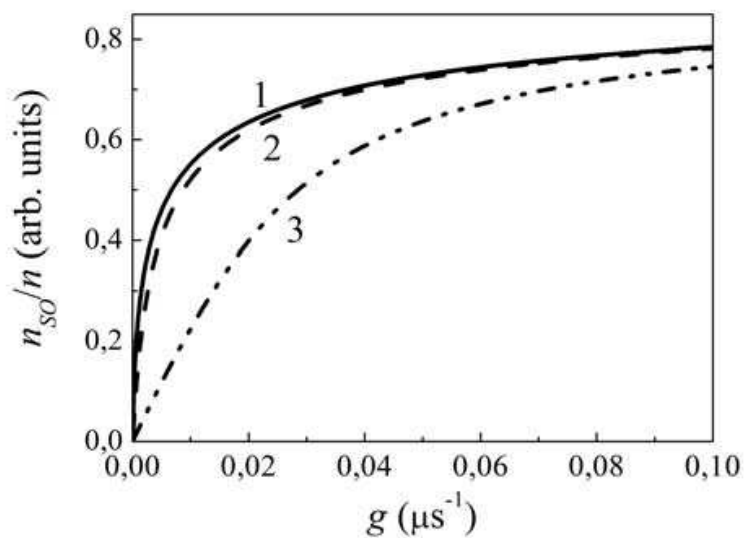

Fig. 11. Calculated dependence of the fraction of photosensitized $^1O_2$ in PS layers on the photoexcitation level at an O_2 molecule concentration n=(1) $2 \cdot 10^{17}$, (2) $2 \cdot 10^{18}$, (3) $2 \cdot 10^{19}$ (3) cm^{-3}.
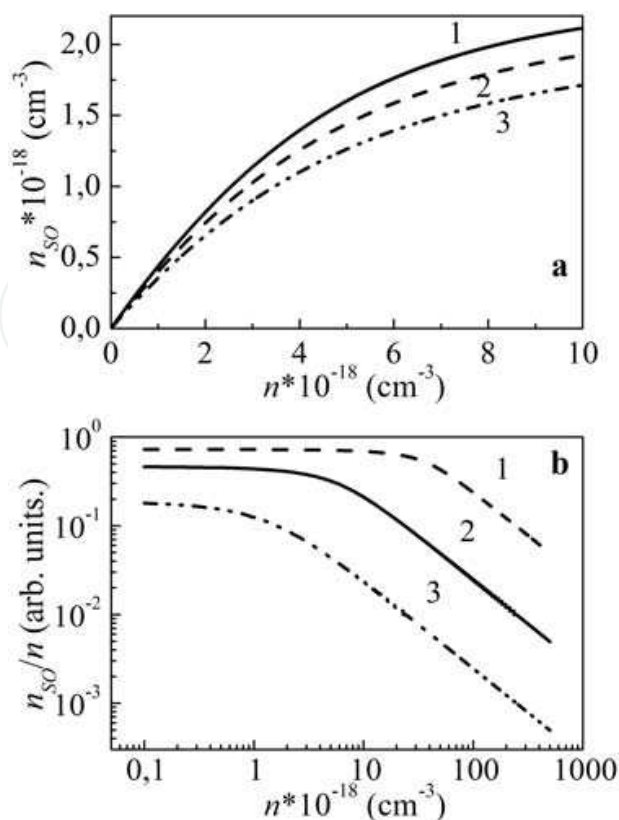
Fig. 12. Calculated dependences illustrating the effect of the molecular oxygen concentration on the $^1O_2$ generation efficiency in PS layers at (a) defect concentration $N'=$(1) 10^{16}, (2) $5 \cdot 10^{16}$, and (3) 10^{17} cm^{-3} and (b) $g=$(1) $5 \cdot 10^{-2}$, (2) $5 \cdot 10^{-3}$, and (3) $5 \cdot 10^{-4}$ µs^{-1}.

Hence, the EPR diagnostics of singlet oxygen generation is inapplicable in the case of a low concentration of O_2 molecules. As noted above, the presence of a defect in a luminescent nc-Si crystal fully suppresses its luminescence due to fast (10^{-9} –10^{-11}) nonradiative trapping of nonequilibrium charge carriers. Therefore, this nanocrystal cannot excite an oxygen molecule on its surface, since the energy transfer time is several tens of microseconds (Gross et al., 2003). This conclusion is reflected in a decrease in the fraction of photosensitized $^1O_2$ when the number of nc-Si crystals with defects increases (Fig. 13). When concentration N' is equal to the number of nc-Si crystals in the ensemble under study (10^{18} cm^{-3}), the $^1O_2$ generation efficiency vanishes (Fig. 13). In the next section, we will show that the calculated dependences have an experimental support.

3.7 Effect of the powder granule size of porous silicon on the luminescence properties

Figure 14 shows micrographs of the FG PS powders taken on a scanning electron microscope. Submicronscale granules are clearly visible apart from micronscale granules (Fig. 14a). Moreover, many microgranules consist of a large number of smaller aggregated particles (Fig. 14b), with the number of such agglomerates increasing with the time of sample storage in air. Indeed, nc-Si crystals in PS layers oxidize in time and their surfaces become hydrophilic. Such PS granules coalesce and form coarse particles due to the
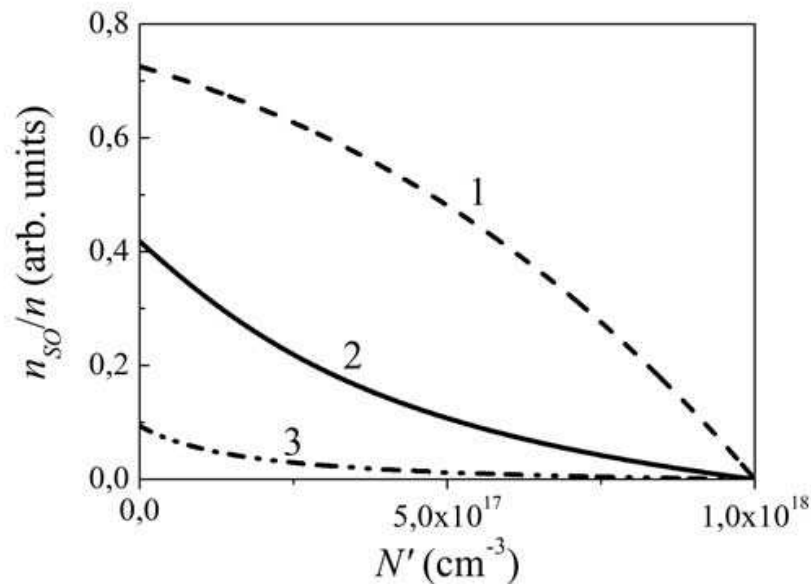
Fig. 13. Calculated dependence of the fraction of photosensitized $^1O_2$ in PS layers on the concentration of nc-Si crystals with defects at g=(1) $5 \cdot 10^{-2}$, (2) $5 \cdot 10^{-3}$, and (3) $5 \cdot 10^{-4}$ μs^{-1}. The O_2 molecule concentration is n=$2 \cdot 10^{17}$ cm^{-3}

hydrogen bonds appearing between them. The image contrast of particles with a diameter of several tens of nanometers in Fig. 14 is low because of their strong static charging. As follows from Fig. 14, simple mechanical milling in a vibratory mill decreases the PS granule size to submicron sizes. This is also indicated by a change in the powder color from dark red–brown (in the case of a CG powder) to light yellow (FG powder), which is likely to be caused by Rayleigh scattering by particles several tens of nanometers in size and structural relaxation (i.e., the relief of microstresses, along which granules predominantly fail). As follows from the EPR spectroscopy data, the concentration of Pb-centers increases almost twofold, from $1.4 \cdot 10^{17}$ to $2.8 \cdot 10^{17}$ cm^{-3}. We assume that this increase leads to a decrease in the PL decay time and, hence, the PL intensity because of an increase in the probability of nonradiative exciton recombination by defects (Delerue et al., 1993).
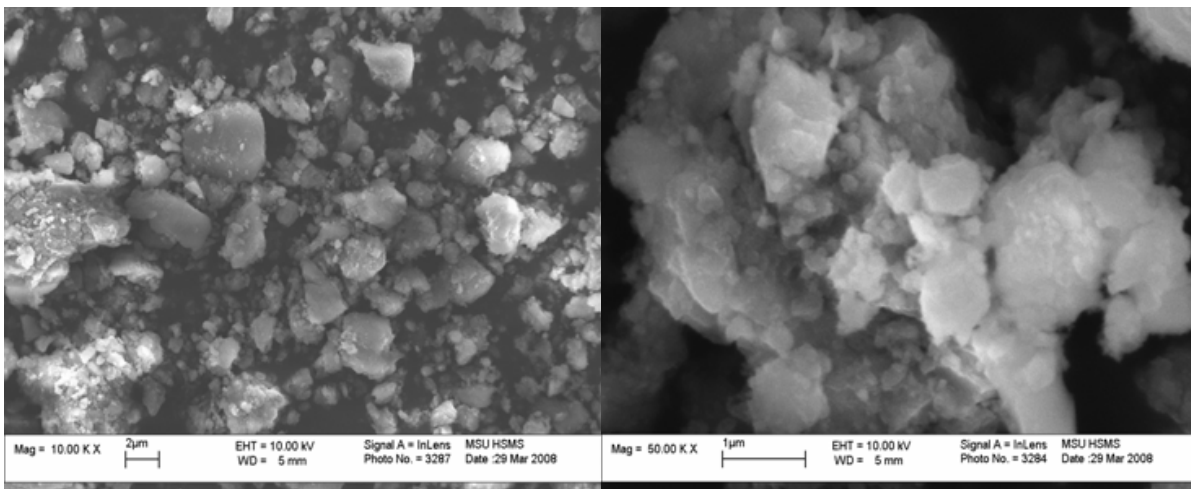

Fig. 14. Scanning electron microscopy micrographs of PS FG powder granules with different scale.

An analysis of the relaxation times demonstrates that, for PS1 samples, they increase in the powders subjected to FG milling (Fig. 15a), which is in conflict with the assumption made above.
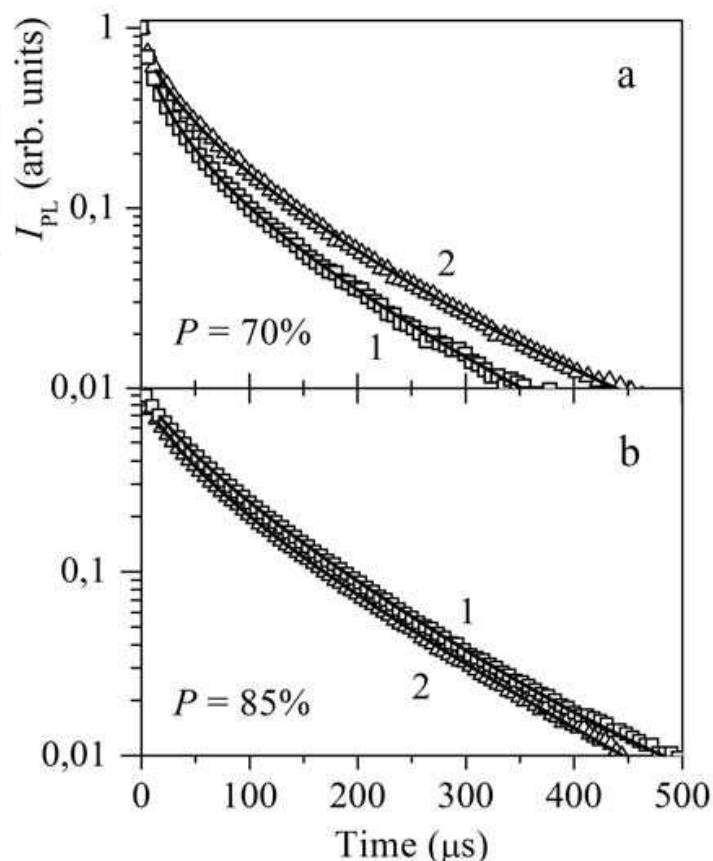

Fig. 15. PL kinetics of (1) CG and (2) FG (a) PS1 and (b) PS2 powders in a vacuum p_{o_2} =1 mbar recorded at a wavelength λ=760 nm. Approximating dependences calculated using the proposed model (solid lines).

This experimental fact can be explained in terms of a model of exciton migration along a network of intersecting nc-Si crystals with a preferred motion direction from smaller to larger crystallites (against the gradient of the energy gap). Both radiative and nonradiative recombination is possible in each of the intermediate nc-Si crystals. The experimental fact of an increase in the PL relaxation time for the FG PS powders as compared to the CG powders can be explained by a decrease in the number of possible exciton migration ways when PS films are milled to granules with sizes varying from several tens to several hundreds of nanometers. For every fraction of nc-Si crystals having a certain size, a nonradiative relaxation channel is partly suppressed due to exciton motion from these nanocrystals; as a result, the exciton lifetimes at the PL wavelength corresponding to this nc-Si crystal size increase. It is important that the properties are modified upon crystal refinement only for nc-Si crystals on a fracture surface and that the internal porous structure of PS granules remains unchanged. Then, the detected change in the PL properties of the samples is related to the fact that the number of surface nc-Si crystals becomes comparable with their number

in the volume of a PS granule when its size decreases from approximately 50 μm (etched layer thickness) to several tens of nanometers. Therefore, this effect can be detected experimentally. Indeed, the simplest model considerations yield the following estimate of the ratio of the number of surface nc-Si crystals having a spherical shape to their number in the volume of a spherical granule: $\varphi = \dfrac{6r}{R}$, where r is the nanocrystal radius and R is the granule radius. Assuming $2r$=3 nm and $2R$ = 90 nm, we find that 20% of all nc-Si crystals that form a PS granule of the given size are at its surface; at $2R$ = 1000 nm, the fraction of surface nc-Si crystals is only about 2%. To test the hypothesis of restricted exciton migration, we prepared samples (PS2) with a higher porosity (85%). At such a high porosity, PS2 nanocrystals are known to be almost completely isolated from each other (Bisi et al., 2000); therefore, exciton migration along an nc-Si network is substantially restricted as compared to the PS1 samples. Thus, milling of PS2 samples should not significantly change their luminescence properties. Indeed, the kinetic curves of a decrease in the PL intensity for the CG and FG PS2 powders are almost the same (Fig. 15b), and the nonexponential segments at short times that are mainly caused by exciton migration are almost absent (cf. Figs. 15a, 15b). The solid lines in Fig. 15 represent approximating dependences calculated by Eq. (22). The table 2 gives the approximation parameters for the kinetic curves that were discussed above (α, $\zeta = 2D^{*}N_{1}^{(0)}$). The relative error in determining these parameters is about 10% and reflects the variation in the values of α and ζ when the approximation range and the initial value of an approximating curve change. Parameter ζ, which describes the migration rate, is seen to decrease upon fine milling of PS1 powders, which indicates a decrease in the efficiency of exciton motion from nc-Si crystals in the ensemble under study. Using the parameters determined in Section 3.4 by Eq. (31), we can calculate migration coefficients D^{*} for CG and FG PS1 samples; they are found to be $3.9 \cdot 10^{13}$ and $1.3 \cdot 10^{13}$ cm³/s, respectively. Thus, upon fine milling of CG PS samples with a porosity of 70%, diffusion coefficient D^{*} averaged over an ensemble of nc-Si crystals decreases approximately threefold. The weak change in parameter α upon fine milling of PS samples indicates a low value of DN' compared to α_{r} (see Eq. (21)) in spite of an approximately twofold increase in the defect concentration. Parameter $\zeta = 2D^{*}N_{1}^{(0)}$ turns out to be higher than α_{r}, which leads to the expected result $N_{1}^{(0)} \gg N'$. Indeed, $N_{1}^{(0)}$ can reach several tens of percent of the number of all nc-Si crystals N for a sufficiently high level of optical excitation (see Fig. 10); then, we have $N_{1}^{(0)} \sim 0.1N \gg N'$. This inequality reflects the following well-known empirical fact: the number of defects is substantially smaller than the number of nc-Si crystals. For example, a fractal model of the PS microstructure yields $N'/N \approx 10^{15}$ cm⁻³ $/10^{18}$ cm⁻³=10^{-3} for the ensemble of nc-Si crystals under study (see Section 3.4). The developed theory can be used to determine the actual radiative PL lifetime of an ensemble of nc-Si crystals, in contrast to formal approximation parameter τ in Eq. (1) for an stretched exponent. Indeed, when analyzing the experimental kinetics, we obtain the value of approximation parameter α_{r}, which is expressed through radiative recombination rate α_{r} ($\alpha \equiv \alpha_{r} + DN'$). As follows from our earlier considerations, DN' is low compared to α_{r} for the as-prepared PS samples; therefore, we can assume $\alpha \approx \alpha_{r}$ for estimation. Another conclusion drawn from an analysis of the approximation parameters of the decrease in the PS PL intensity consists in the fact that all assumptions regarding the smallness of the terms describing exciton migration as

compared to nonradiative recombination rate α' for luminescent nc-Si crystals are justified. Indeed, these kinetic curves were obtained at a wavelength $\lambda = 760$ nm, which corresponds to $E_g \approx 1.6$ eV. At this energy gap, the characteristic rate of nonradiative recombination at a defect is more than 10^4 μs^{-1} (Delerue et al., 1993), whereas the exciton migration rate $\zeta = 2D^*$ is no more than 0.04 μs^{-1}. Therefore, any products of type DN are substantially lower than α' even if the total number of nc-Si crystals is larger than the number of initially excited nanocrystals ($N > N_1^{(0)}$).

3.8 Effect of the degree of oxidation on the photosensitization activity of porous silicon

To study the efficiency of $^1O_2$ generation on the nc-Si surface, it is important to know its dependence on the photostimulated oxidation of PS samples during the photosensitization of molecular oxygen. Figure 16a shows the EPR spectra of coarse-grained PS1 powders that were recorded in an oxygen atmosphere as a function of the exposure time during irradiation by the light of a galogen lamp. The spectrum amplitude (and P_b-center concentration, respectively) is seen to monotonically increase with exposure time t_{exp} (Fig.16b). For PS powders to be applied in photodynamic therapeutic methods, it is

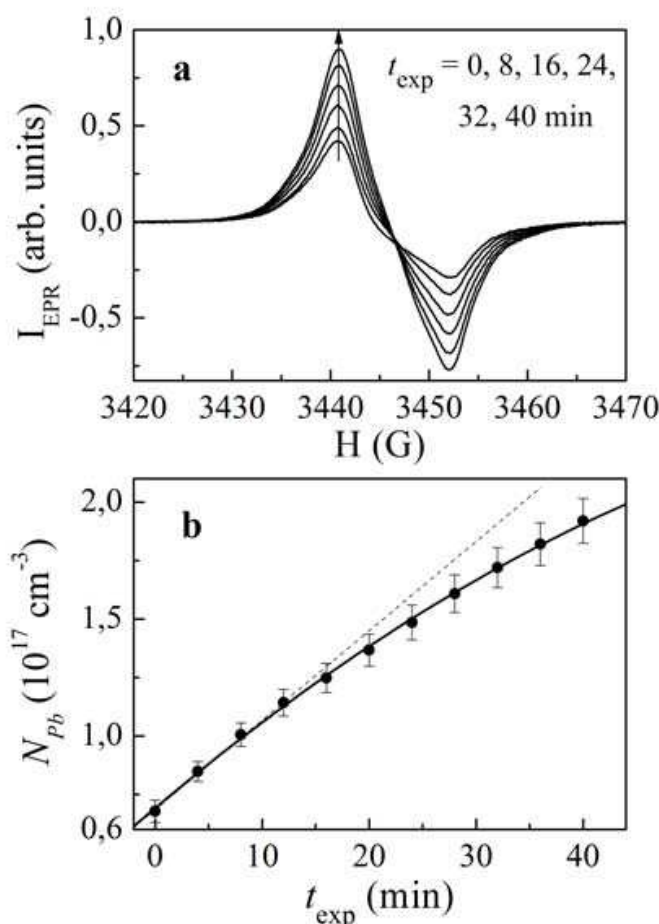Fig. 16. (a) EPR spectra of PS1 powders and (b) the corresponding concentrations of P_b-centers as a function of exposure time t_{exp} in an O_2 atmosphere. (b): (solid line) for clarity and (dashed line) linear dependence at P_{mw}=2.0 mW.

important to study the effect of the number of defects on the efficiency of singlet oxygen generation. Figure 17a shows the PL spectra of CG PS1 powders recorded in vacuum at various times t_{exp} of preliminary holding under the light in an oxygen atmosphere. The PL intensity decreases monotonically according to an increase in the contribution of nonradiative recombination, and the spectral maximum shifts toward short wavelengths due to an increase in the quantum confinement of excitons in Si nanostructures upon an increase in the surface SiO_2 oxide thickness (Bisi et al., 2000).
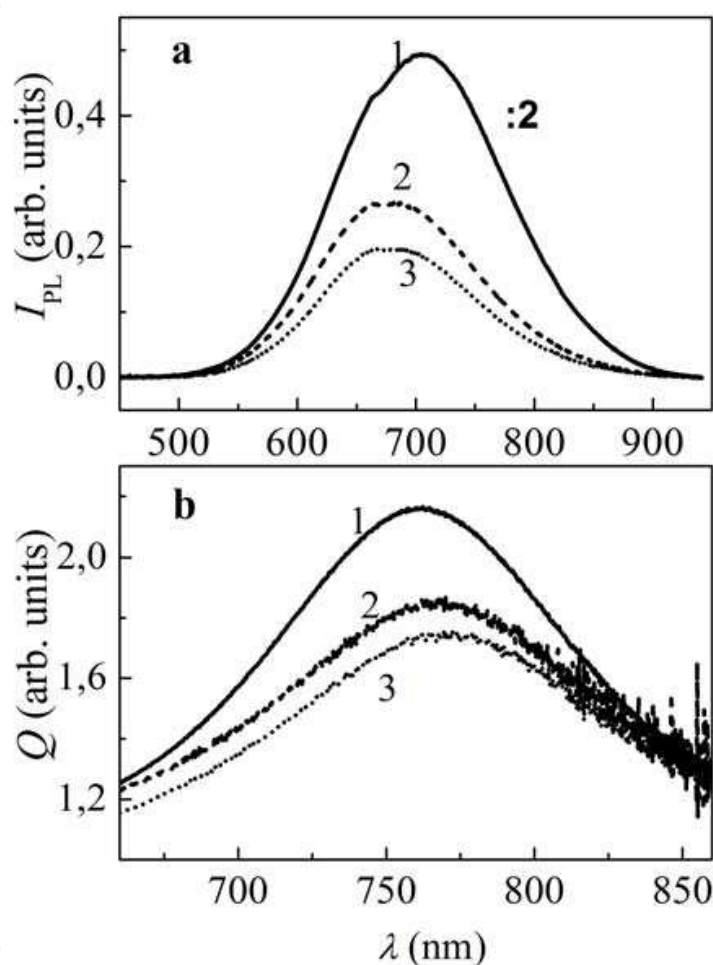
Fig. 17. (a) PS1 PL spectra and (b) quenching function $Q(\lambda)$ during illumination in an O_2 atmosphere at t_{exp}= (1) 0, (2) 6, and (3) 12 min.

Using the dependence of the concentration of P_b-centers in an ensemble of nc-Si crystals on the exposure time as a normalized curve (Fig. 16b), we can plot the dependence of the PL intensity at a certain wavelength on the defect concentration (Fig. 18a). The curve in Fig. 18a is seen to agree quantitatively with the calculated curves in Fig. 10a, which indicates that the initial principles of the developed exciton migration theory are consistent.

When the number of defects increases, the $^1O_2$ generation efficiency degrades, which is indicated by the monotonic decrease in the quenching function amplitude $Q(\lambda) = I_{PLvac}/I_{PLair}$ air with increasing time t_{exp} (Fig.17b). The quenching function is the ratio of the PS PL spectrum amplitudes in vacuum and an oxygen-containing medium and

characterizes the intensity of exciton recombination followed by energy transfer to oxygen molecules (Gross et al., 2003). Note that the quantity

$$1 - Q^{-1} = \frac{I_{vac} - I_{air}}{I_{vac}} \tag{36}$$

approximately determines the fraction of oxygen molecules in the singlet state on the assumption that the entire energy of PL quenching of PS samples is consumed for the excitation of molecular oxygen.
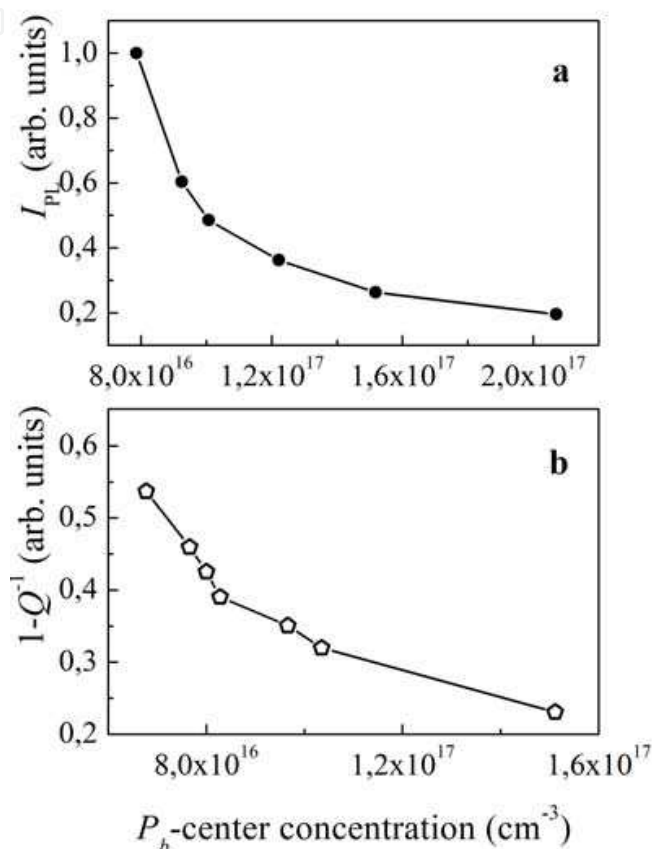

Fig. 18. Effect of the defect concentration on the PL intensity (λ=740 nm) and the fraction of photosensitized O_2 (λ=760 nm). The dependences were obtained upon processing the data some of which are shown in Fig. 17.

Figure 18b shows quantity (36) as a function of the concentration of the defects that form during photostimulated oxidation at a wavelength λ=760 nm. The photosensitized activity of PS layers is seen to monotonically decrease with increasing number of P_b-centers, which points to the suppression of the luminescent and, hence, photosensitized properties of nanocrystals with point defects. As in the case of the PL intensity, the calculated curves shown in Fig. 13 agree qualitatively with the experimental curve in Fig. 18b. Thus, the photostimulated oxidation of PS samples leads to a monotonic decrease in the $^1O_2$ generation efficiency, which is important for practical application. After photosensitization, ensembles of nc-Si crystals transform into harmless amorphous SiO_2, which does not exert a phototoxic effect on biological tissues.

4. Conclusions

The generation of singlet oxygen was investigated and its concentration upon photoexcitation of silicon nanocrystals in microporous silicon layers was determined using EPR spectroscopy. It was demonstrated that a considerable part (approximately 40%) of the molecules of triplet oxygen can transform into the singlet state in the course of photosensitization of oxygen molecules in ensembles of silicon nanocrystals. The longitudinal (T_1) and transverse (T_2) relaxation times of spin centers increase under illumination of the samples in an oxygen atmosphere owing to the decrease in the efficiency of the dipole–dipole interaction between silicon dangling bonds and molecules of triplet oxygen as a result of the transformation of a number of the latter molecules into an excited (diamagnetic) state. It was shown that the amplitude of the EPR spectrum of triplet oxygen molecules in pores of silicon decreases upon photoexcitation of the samples, which suggests the formation of singlet oxygen molecules.

Taking into account exciton migration, we developed a quantitative model for the relaxation processes that occur in ensembles of silicon nanocrystals. With this model, we theoretically described the photosensitization of singlet oxygen on the surface of silicon nanocrystals under various external conditions. We experimentally studied the effect of the granule size of a porous silicon powder on its luminescence properties. Upon mechanical fine milling of as-deposited PS films, both the PL intensity and the concentration of point defects increase. The effect of the photostimulated oxidation of PS layers on the photosensitization of molecular oxygen on the surface of the nanocrystals forming the PS was investigated. The photosensitized activity of silicon nanocrystals was found to degrade monotonically during their oxidation. With the developed model, we explained the experimental data by restricted energy transfer between coupled silicon nanocrystals because of breaks in exciton migration trajectories when the granule size of a PS powder decreases and by an increase in the efficiency of nonradiative recombination during the photostimulated oxidation of the nanocrystals, which leads to the suppression of singlet oxygen generation. Moreover, using this model, we can approximate the kinetic curves of PL decay at a high accuracy, determining the actual exciton radiative recombination time in the nanocrystals. Our data indicate that PS is promising for the methods of nontoxic photodynamic therapy of a number of diseases, including oncological ones.

5. Acknowledgment

6. References

Bisi, O.; Ossicini, S. & Pavesi, L. (2000). *Porous Silicon: a Quantum Sponge Structure for Silicon Based Optoelectronics. Surface Science Reports*, Vol.38, No.1-3, (April 2000), p.p. 1-126, ISSN 0167-5729.

Cantin, J.; Schoisswohl, M.; Bardeleben, H.; Hadj, N. & Vergnat, M. (1995). *Electron-Paramagnetic-Resonance Study of the Microscopic Structure of the Si (100)-SiO2 Interface.*

Physical Review B: Condensed Matter, Vol.52, No.16, (April 1995), p.p. R11599-R11602, ISSN 1098-0121.

Carrington, A. & McLachlan, A. (1979). *Introduction to Magnetic Resonance with Applications to Chemistry and Chemical Physics*, Chapman and Hall, ISBN 047026572, New York, United States of America.

Chen, R. (2003). *Apparent Stretched-Exponential Luminescence Decay in Crystalline Solids.* Journal of Luminescence, Vol.102–103, (May 2003), p.p. 510-518, ISSN 0022-2313.

Chen, X.; Henderson, B. & O'Donnell, K. (1992). *Luminescence Decay in Disordered Low-Dimensional Semiconductors.* Applied Physics Letters, Vol. 60, No.21, (March 1992), p.p. 2672-2674, ISSN 0003-6951.

Cullis, A. & Canham, L. (1991). *Visible Light Emission due to Quantum Size Effects in Highly Porous Crystalline Silicon.* Nature, Vol.353, No. 6342, (August 1991), p.p. 335-338, ISSN 0028-0836.

Delerue, C.; Allan, G. & Lannoo, M. (1993). *Theoretical Aspects of the Luminescence of Porous Silicon.* Physical Review B: Condensed Matter, Vol.48, No.15, (October 1993), p.p. 11 024-11036, ISSN 1098-0121.

Dexter, D. (1953). *A Theory of Sensitized Luminescence in Solids. Journal of Chemical Physics*, Vol.21, (September 1953), p.p. 836-850, ISSN 0021-9606.

Germanenko, I.; Li, S. & El-Shall, M. (2001). *Decay Dynamics and Quenching of Photoluminescence from Silicon Nanocrystals by Aromatic Nitro Compounds.* Journal of Physical Chemistry B, Vol.105, No.1, (January 2001), p.p. 59-66, ISSN 1520-6106.

Gross, E.; Kovalev, D.; Künzner, N.; Diener, J.; Koch, F.; Timoshenko, V. & Fujii, M. (2003). *Spectrally Resolved Electronic Energy Transfer from Silicon Nanocrystals to Molecular Oxygen Mediated by Direct Electron Exchange.* Physical Review B: Condensed Matter, Vol.68, No.11, (September 2003), p.p. 115405-1-115405-11, ISSN 1098-0121.

Hahn, E. (1950). *Spin Echoes.* Physical Review, Vol.80, No.4, (November 1950), p.p. 580-594, ISSN 1098-0121.

Halliwell, B. & Gutteridge, J. (1999). *Free Radicals in Biology and Medicine*, 3th ed., Oxford University Press, ISBN 0-19-850044-0, Oxford, United Kingdom.

Kanemitsu, (1996). *Photoluminescence Spectrum and Dynamics in Oxidized Silicon Nanocrystals: Nanoscopic Disorder System.* Physical Review B: Condensed Matter, Vol.53, No.11, (September 1996), p.p. 13513-13520, ISSN 1098-0121.

Kovalev, D.; Gross, E.; Künzner, N.; Koch, F.; Timoshenko, V. & Fujii, M. (2002). *Resonant Electronic Energy Transfer from Excitons Confined in Silicon Nanocrystals to Oxygen Molecules.* Phys. Rev. Lett. Vol.89, No.13, (September 2002), p.p. 137401-1-137401-4, ISSN 0031-9007.

Kumar, V.; Tripathi, M.; Kumar, M. & Shukla, G. (2009). *Photosensitization Studies in Selected Dyestuffs.* E-Journal of Chemistry, Vol. 6, No.3, (Juli, 1999), p.p. 659-664, ISSN 0973-4945.

Laiho, R.; Vlasenko, L.; Afanasiev M. & Vlasenko, M. (1994) *Electron Paramagnetic Resonance in Heat-Treated Porous Silicon.* Journal of Applied Physics, Vol.76, No.7, (June 1994), p.p. 4290-4293, ISSN 0021-8979.

Lebib, S.; Bardeleben, H.; Cernogora, J.; Fave, J. & Roussel, J. (1999). *Time-Resolved Photoluminescence Study of the Red Emission in Nanoporous SiGe Alloys.* Journal of Luminescence, Vol.80, No.1-4, (March 1999), p.p. 153-157, ISSN 0022-2313.

Lepine, D. (1972). *Spin-Dependent Recombination on Silicon Surface.* Physical Review B: Solid State Vol.6, No.2, (July 1972), p.p. 436-441, ISSN 1098-0121.

Linnros, J.; Lalic, N.; Galeckas, A. & Grivickas, V. (1999). *Analysis of the Stretched Exponential Photoluminescence Decay from Nanometer-Sized Silicon Crystals in SiO₂.* Journal of Applied Physics, Vol.86, No.11, (August 1999), p.p. 6128-6134, ISSN 0021-8979.

Maly, F.; Trojanek, P.; Kudma, J.; Hospodkova, A.; Banas, S.; Kohlova, V.; Valenta, J.; & Pelant, I. (1996). *Picosecond and millisecond dynamics of photoexcited carriers in porous silicon.* Physical Review B: Condensed Matter, Vol.54, No.11, (September 1996), 7929-7936, ISSN 1098-0121.

Mihalcescu, I.; Vial, J. & Romestain, R. (1996). *Carrier Localization in Porous Silicon Investigated by Time-Resolved Luminescence Analysis.* Journal of Applied Physics, Vol.80, No.4, (May 1996), p.p. 2404-2411, ISSN 0021-8979.

Moretti, L.; De Stefano, L. & Rendina, I. (2007). *Quantitative Analysis of Capillary Condensation in Fractal-Like Porous Silicon Nanostructures.* Journal of Applied Physics, Vol.101, No.2, (January 2007), p.p. 024 309-1-024 309-5, ISSN 0021-8979.

Nychyporuk, T.; Lysenko, V. & Barbier, D. (2005). *Fractal Nature of Porous Silicon Nanocrystallites.* Physical Review B: Condensed Matter, Vol.71, No.11, (March 2005), p.p. 115 402-1-115 402-5, ISSN 1098-0121.

Pavesi, L. & Ceschini, M. (1993). *Stretched-Exponential Decay of the Luminescence in Porous Silicon.* Physical Review B: Condensed Matter, Vol.48, No.23, (December 1993), p.p. 17625-17628, ISSN 1098-0121.

Poole, C.P. & Horacio, F. (1987). *Theory of Magnetic Resonance, 2nd Ed.*, Wiley, ISBN: 978-0-471-81530-3C, New York, United States of America.

Pophristic, M.; Lang, F.; Tran, C.; Ferguson, I. & Karlicek, R. (1998). *Time-Resolved Photoluminescence Measurements of InGaN Light-Emitting Diodes.* Applied Physics Letters, Vol.73, No.24, (October 1998), p.p. 3550-3552, ISSN 0003-6951.

Proot, J.; Delerue, C. & Allan, G. (1992). *Electronic Structure and Optical Properties of Silicon Crystallites: Application to Porous Silicon.* Applied Physics Letters, Vol.61, No.16 , (August 1992), p.p. 1948-1950, ISSN 0003-6951.

Roodenko, K.; Goldthorpe, I.; McIntyre, P. & Chabal, Y. (2010). *Modified Phonon Confinement Model for Raman Spectroscopy of Nanostructured Materials.* Physical Review B: Condensed Matter, Vol.82, No.11, (September 2010), p.p. 115210-1-115210-11, ISSN 1098-0121.

Smith, R. & Collins, S. (1992). *Porous Silicon Formation Mechanisms.* Journal of Applied Physics, Vol. 71, No.8, (January 1992), p.p. R1-R22, ISSN 0021-8979

Vahtras, O.; Loboda, O.; Minaev, B.; Ågren H. & Ruud K. (2002). *Ab Initio Calculations of Zero-Field Splitting Parameters.* Chemical Physics, Vol.279, No.2-3, (June 2002), p.p. 133-142, ISSN 0301-0104.

Vinciguerra, V.; Franzo, G.; Priolo, F.; Iacona, F. & Spinella, C. (2000). *Quantum Confinement and Recombination Dynamics in Silicon Nanocrystals Embedded in Si/SiO₂ Superlattices.* Journal of Applied Physics, Vol.87, No.11, (February 2000), p.p. 8165-8173, ISSN 0021-8979.
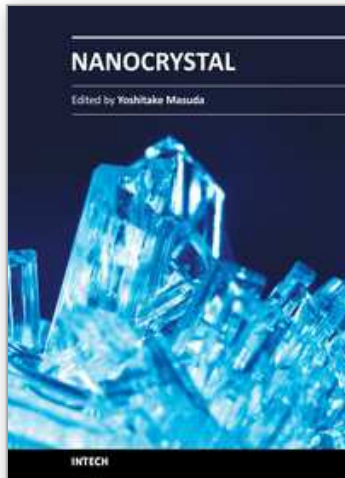
Nanocrystal

Edited by Dr. Yoshitake Masuda

We focused on cutting-edge science and technology of Nanocrystals in this book. "Nanocrystal" is expected to lead to the creation of new materials with revolutionary properties and functions. It will open up fresh possibilities for the solution to the environmental problems and energy problems. We wish that this book contributes to bequeath a beautiful environment and valuable resources to subsequent generations.

How to reference

In order to correctly reference this scholarly work, feel free to copy and paste the following:

INTECH

open science | open minds